

Utilizing Advanced Spatial Collection and Monitoring Technologies:
Surveying Topographical Datasets with Unmanned Aerial Systems

by

Charles R. Jurden, Jr.

A Thesis Presented to the
Faculty of the USC Graduate School
University of Southern California
In Partial Fulfillment of the
Requirements for the Degree
Master of Science
(Geographic Information Science and Technology)

May 2018

To my family, Jennifer, Alexis, Zakary, Emma-Grace, and Mila Jade.

Table of Contents

| | |
|--|------|
| List of Figures | vi |
| List of Tables | vii |
| Acknowledgements | viii |
| List of Abbreviations | ix |
| Abstract | xii |
| Chapter 1 Introduction | 1 |
| 1.1. Motivation | 1 |
| 1.2. Data | 3 |
| 1.2.1 Study Areas | 4 |
| 1.3. Collections Methods | 6 |
| Chapter 2 Related Works | 9 |
| 2.1. Lineage | 9 |
| 2.2.1 Data Use | 10 |
| 2.2. History | 10 |
| 2.3. Relative Research | 11 |
| 2.4. Precision and Accuracy Analysis Methods | 13 |
| 2.4.1 Formula | 13 |
| Chapter 3 Data and Methods | 18 |
| 3.1. Comparative Data | 18 |
| 3.2. Pre-Flight Planning | 18 |
| 3.3. Project Flight | 21 |
| 3.3.1 Flight Parameters | 21 |
| 3.3.2 Study Areas | 24 |

| | |
|---|----|
| 3.3.3 Scale and the Lens | 25 |
| 3.3.4 Tallgrass Site Flight Pattern | 26 |
| 3.3.5 Asphalt Site Flight Pattern | 28 |
| 3.3.6 Dickinson Site Flight Pattern | 29 |
| 3.4. Data Extraction and Processing | 29 |
| 3.5. Accuracies..... | 31 |
| Chapter 4 Results | 37 |
| 4.1. Results Analysis..... | 37 |
| 4.2. Individual Site Results | 40 |
| 4.2.1 Asphalt Site | 40 |
| 4.2.1 Dickinson Site | 41 |
| 4.2.3 Tallgrass Site | 43 |
| 4.3. Confidence Levels | 44 |
| Chapter 5 Discussion and Conclusions..... | 48 |
| 5.1. SWOT (Strengths Weaknesses Opportunities Threats) Analysis | 48 |
| 5.1.1 Strengths..... | 48 |
| 5.1.2 Weaknesses | 49 |
| 5.1.3 Opportunities..... | 50 |
| 5.1.4 Threats | 50 |
| 5.2. Sources of Error and Problems | 51 |
| 5.3. Future Improvements | 52 |
| References..... | 55 |
| Appendix A Tables and Maps..... | 61 |

List of Figures

| | |
|--|----|
| Figure 1 OGRIP LiDAR point cloud | 2 |
| Figure 2 Scale & focal length interepretation | 15 |
| Figure 3 Trigonomic function of aerial triangulation | 16 |
| Figure 4 Flight parameters created in DJI GSP at the Tallgrass Site..... | 20 |
| Figure 5 Tallgrass GCP placement location | 27 |
| Figure 6 Asphalt site volume map | 68 |
| Figure 7 Asphalt site contour map – P 1 | 69 |
| Figure 8 Asphalt site contour map – P 2 | 70 |
| Figure 9 Asphalt site contour map – P 3 | 71 |
| Figure 10 As-Built compilation report – Price Pad P 1 | 72 |
| Figure 11 As-Built compilation report – Price Pad P 2 | 73 |
| Figure 12 Tallgrass site As-built/UAS comparison map | 74 |
| Figure 13 LiDAR/LAS comparison chart 1 | 75 |
| Figure 14 LiDAR/LAS comparison chart 2..... | 76 |

List of Tables

| | |
|---|----|
| Table 1 GCP report for accuracy | 25 |
| Table 2 GCP comparison chart | 32 |
| Table 3 Inversion report | 32 |
| Table 4 LiDAR report chart | 34 |
| Table 5 Absolute camera and deviation uncertainties | 38 |
| Table 6 Relative geolocation variance report for the Asphalt site | 39 |
| Table 7 Asphalt random samples | 41 |
| Table 8 Dickinson random samples | 42 |
| Table 9 Tallgrass random samples (A) | 43 |
| Table 10 Tallgrass random samples (B) | 44 |
| Table 11 Deviation report | 45 |
| Table 12 Root Mean Square/Altitude relationship table | 65 |
| Table 13 USGS check shot point | 65 |
| Table 14 LAS points derived from UAS | 66 |
| Table 15 Data sources | 67 |

Acknowledgements

I am grateful for the support of my family throughout this grand adventure. Through the time that it has taken to complete this part of our journey, we have found struggles and the patience to persevere, we found elations and imprinted them upon our hearts. I am thankful to the staff of USC's Dornsife for their guidance and unmatched skill in their disciplines. Fight on!

List of Abbreviations

| | |
|-------|--|
| AGL | Above Ground Level |
| ASPRS | American Society for Photogrammetry and Remote Sensing |
| cm | centimeter |
| C.I. | Contour Interval |
| csv | comma separated value |
| DEM | Digital Elevation Model |
| DSM | Digital Surface Model |
| DTM | Digital Terrain Model |
| FAA | Federal Aviation Administration |
| ft | foot |
| GCP | Ground Control Point |
| GIS | Geographic information system |
| GISci | Geographic information science |
| GNSS | Global Navigation System |
| GPS | Global Positioning System |

| | |
|----------|---|
| GRD | Ground Resolve Distance |
| GRS80 | Geodetic Reference System 1989 |
| GSD | Ground Sampling Distance |
| HDOP | Horizontal Dilution of Precision |
| in | inch |
| INS | Inertial Navigation System |
| jpg | digital image (Joint Photographic Experts Group format) |
| LAS | Laser file format (LiDAR exchange files) |
| LiDAR | Light Detection and Ranging |
| m | meter |
| Micro SD | Micro Secure Digital data storage card |
| MPH | Miles Per Hour |
| NAD83 | North American Datum 1983 |
| NAVD88 | North American Vertical Datum 1988 |
| ODOT | Ohio Department of Transportation |
| OGRIP | Ohio Geographically Referenced Information Program |

| | |
|------|---|
| OSIP | Ohio Statewide Imagery Program |
| P4 | DJI Phantom 4 |
| P4D | Pix4D software |
| PDOP | Position Dilution of Precision |
| px | pixel |
| RMSE | Root Mean Square Error |
| RPIC | Remote Pilot in Charge |
| RTK | Real-Time Kinematic |
| tif | Tagged Image File |
| TIN | Triangulated Irregular Network |
| UAS | Unmanned Aerial System |
| USC | University of Southern California |
| USGS | United States Geological Survey |
| VDOP | Vertical Dilution of Precision |
| VRS | Virtual Reference System |
| XYZ | Longitude – Latitude (or, Easting – Northing) and Vertical (respectively) |

Abstract

This study detailed the data collection, processing, and source comparison of DJI Unmanned Aerial System (UAS) drone data from different examples of topographical datasets for accuracy testing. Three datasets were chosen as they were characteristically different, these terrains were those typically encountered while surveying in the energy industry and are representative of terrain types encountered in the south Ohio area. More broadly they are comparable with other terrain systems.

The system used to collect the UAS data consisted of a DJI Phantom 4 unmanned aerial vehicle controlled by DJI Ground Station Pro on an iPad Pro that input and monitored flight parameters. The processing used various software applications. These included Pix4D, which was the photogrammetry software used to convert the data into georeferenced mosaics, models, and point clouds. Additionally, Esri's ArcGIS and Idrisi Terrset were also used in performing analysis.

The data was then analyzed to find correlation to LiDAR and ground control to compare elevation similarities. For the purpose of this study ground control points and LiDAR are considered the trusted source of reference accuracy and precision. Accuracy was assessed against the control material by inversion methods, geometry, and visual assessments. The testing concluded cohesive data precision, accuracy, and detailed the process of creating remotely-sensed materials and their conversion to geometrically accurate data.

Chapter 1 Introduction

Technological advances using drones in Unmanned Aerial Systems for spatial data acquisition and the subsequent software processing programs that are used for topographical surveying in large-scale mapping projects increase resource usability while maintaining accuracy and precision. This research was directed at comparing the output of drone collected data to aerial methods that are already a source of data trusted by mapping organizations. This work evaluated the success of large-scale topographical projects.

1.1. Motivation

The test areas that were chosen and surveyed were sites that covered fifteen or less acres, had different terrain types, and represented potential various stages in the construction phases of the energy industry. Topographic data in the survey field is historically collected using time-consuming, conventional measures that incorporate a total station, transit, level, or theodolite, or with GPS technology. None of these methods have imagery (that helps the office technician or processing agent) through providing an overview of surveyed land areas, minus a field book of notes there are no cross-referenced ‘of the date surveyed’ materials. Online satellite imagery is available, from sites such as Google Earth – but it is not up-to-date with the features that are present on the day an area is surveyed. Many times, structures and/or features are new or absent in the imagery, which ultimately renders these sources obsolete.

This study focused on the collection of this type of data using a drone (Unmanned Aerial Systems [UAS]) remote sensing image capture and support software with the capacity to capture precise and accurate photogrammetric data. This potentially may become the standard source for

data retrieval in future survey, as well as the context for producing digital elevation models (DEM), point clouds, and Orthomosaic imagery.

1.1.2 LiDAR

LiDAR is the acronym for “Light Detection and Ranging.” Its technology uses lasers to transmit and receive energy frequencies in phase and of narrow range to form images (Campbell & Wynne, 2011). It is also referred to as airborne laser altimeter, where the echoes created by the laser pulsing from its aerial host acquires point data by return measures. The return data is dense, meaning that there is an immense amount of collected points containing XYZ data. X data is longitudinal, Y is latitudinal, and Z data is height above the earth’s surface. The output is in the form of point clouds, with the higher elevations having lighter colors to indicate Z, and gradually darkening as Z lowers in elevation (see Figure 1).

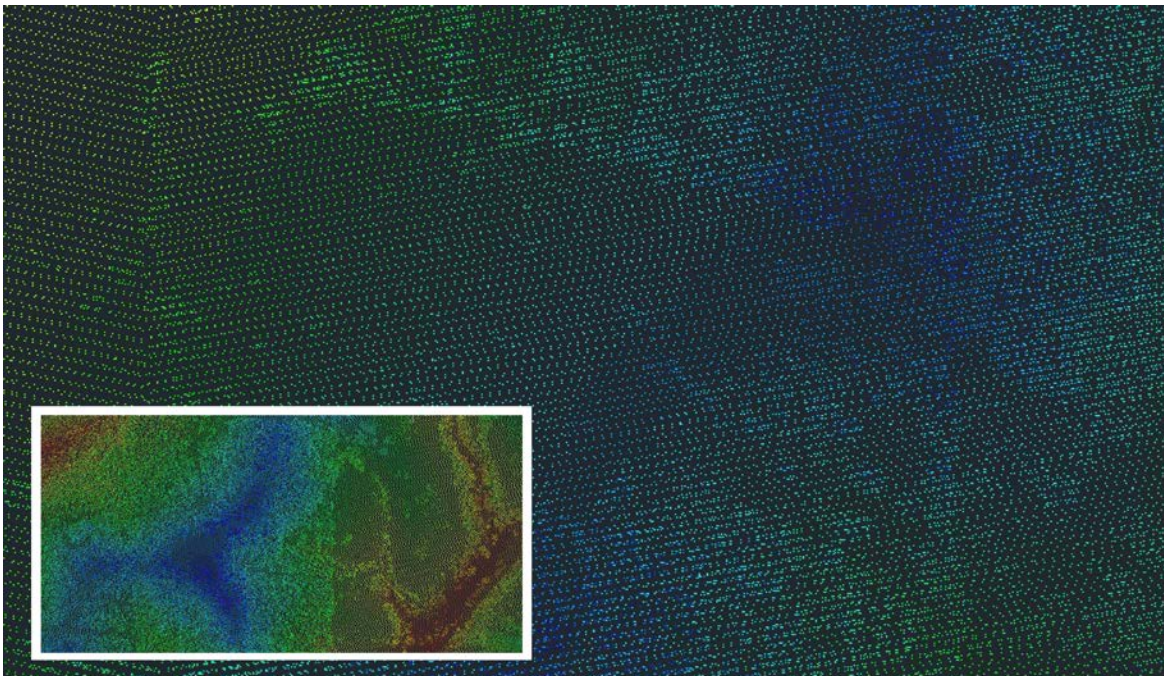


Figure 1 OGRIP LiDAR point cloud.

1.2. Data

The Remote Pilot in Charge (or, RPIC) collected datasets from three sites using a drone. They were then compared with those collected from LiDAR and as-generated as-built data. These LiDAR data are considered “trusted” as being accurate according to the American Society of Professional Remote Sensing (McGlone, Chris, 2014). ASPRS established Accuracy Standards for Digital Geospatial Data and is considered the authority of survey standards for aerially recorded and processed data. Processed data resulted in similar topographical output, and the comparisons concluded cohesive data precision to that of geometrically accurate data.

This study defined advantages of automated digital photogrammetry by concluding that the multi-scale applicability allowed the “creation of coherent standard grid-based digital elevation models (DEMs) of consistent precision and at very high sampling rates, thus able to record very detailed morphology” (Walstra, J., Chandler, J., Dixon, N., Dijkstra, T., n.d.).

In this research, the acquisition of drone related aerial photography used the following considerations:

- *Ground coverage* – The areas of interest were completely covered by the stereoscopic overlap area of the images, with extended spectral range that could detect wavelengths beyond the typical human ability.
- *Scale* – The scale of the photographs determine what precision photo-coordinates were measured and feature sizes were discerned.

- *Digital Elevation Model (DEM) creation* - The digital representation of terrain was created from Digital Terrain Models (DSMs) processed to Digital Surface Models (DSMs) and point clouds were created.
- *Hardware and software performance* – Observations were made into the processing speeds and functionality of the elements of the UAS (as, the unit was a system comprised of various machines), and how improvements could be made (Pix4D, 2017).

1.2.1 Study Areas

The three datasets that were collected were representative of the types of terrain that are typically encountered when surveying large scale multi-acre properties. As well, the variables in these areas supported construction processes of sectors in the energy industry. The first area was a pipeline compressor pad constructed atop a hill, referred to in this thesis as the “Tallgrass Compressor Site”, or (Tallgrass Site). It is a completed facility, housing five large compressor engines in four housing units. The history of the site includes a preliminary topography that was reformed prior to construction. A compressor site consists of several machines that are used to increase pressure along a pipeline, thus enabling product to continue along the pipeline over longer distances with higher pressure. It has multiple buildings and piping networks, masking some areas which created the potential to lose sight of the ground and make measurement difficult.

The second test site was an asphalt mixing plant with multiple stockpiles of rock – referred to in this thesis as the “Asphalt Plant Site”, and was chosen because the area is representative of sites that require stockpile area volume calculation. Different sectors of the

energy field use stockpiles. Coal mining stockpiles product, as did this asphalt plant. The piles are used, and then replaced – creating a need for monitoring product. Others may use stockpiles for “spoil”, which is dirt temporarily removed to clear for trenching. This flyover was used to calculate the volumes of asphalt, which could then be stored in a GIS and compared with quarterly usage to develop trends or monitor loss. The comparative dataset for this project was LiDAR retrieved from the State of Ohio’s online data dump.

The third area was a small lake flyover that consisted of approximately 10 acres of lake and land coupled with steep elevation changes. It was referred to in this report as the “Dickinson Ranch Site”, and was used as a test subject for water reflectance and edge detection to be processed through Idrisi. It was also characterized by the steep elevation changes and heavy vegetation, which, in some instances, have caused incorrect elevation readings. This test region explored various methods for alleviating this error.

The principal goal of this study was to present the output of the photogrammetric image matching topographical dataset from the drone collection. These dataset formats compared favorably with traditional methods of aerial point cloud collection did correlate as datasets of accuracy with precision consistencies. The system used to collect the UAS data consisted of a DJI Phantom 4 unmanned aerial vehicle controlled by DJI Ground Station Pro on an iPad Pro to set flight parameters. The processing of the finished product used various software applications including Pix4D. This software is used to convert the data into georeferenced mosaics, models,

and clouds. Esri ArcGIS ArcMap 10 was used to analyze the DEMs (in the form of DTM and DSM). Idrisi Terrset was utilized in analyzing DEM raster sets for histogram accuracies.

As noted, three datasets were collected from a drone and compared with those collected from trusted sources of satellite captured LiDAR. This thesis aimed at concluded that processing the information collected from the UAS would result in equal or more accurate and precise topographical output when compared to analysis data, and therefore create preference for situations requiring aerial data in the energy sector for mapping, reporting, and planning.

1.3. Collections Methods

Accuracy, the difference between measured and actual value and precision, the difference in the variation between multiple measures of the same object were required for data assessment. Accuracy was not assumed based on programming defaults, but incorporated techniques including ground control points collected with Trimble R8-3 GNSS survey-grade equipment in the NAD 83, Ohio South coordinate system elevation data. From this data, the implementation of Ground Control Points (GCP) measured from a different source than the aerial photography ensured consistency. Ground control points add redundancy to data and provability to statistical analysis. Typical surveying adjustment methods include the compass rule, transit rule, and least squares rule. The compass rule adjusts for equal precision in angular and horizontal error. The transit rule adjusts angular and horizontal errors, but expects that that horizontal angles are measured with higher precision. The least squares method is statistical by nature, and uses various standard deviation formulas to compute best-fit solutions. If any errors occurred in the data when collecting the conventional-type information, the previously mentioned survey adjustment corrections would be utilized.

The different datasets were cross-referenced with other sources at their corresponding locations in the testing areas to compare results for consistency. The Compressor Site was compared to data collected from an as-built survey completed in the beginning of 2015. The Asphalt Plant Site was compared with LiDAR derived from the ohio.gov website (ogrip.oit.ohio.gov, 2017). The Dickinson Site was compared with a ground survey using VRS RTK GNSS GPS recorded in 2017.

The parameters used for the drone flights were consistent in overall pattern, meaning that the flights were performed at two height patterns and used multiple ground control points spread throughout the test area. The asphalt stockpile and the lake's parameters were similar.

Data accuracy was measured against national standards, determined by horizontal and vertical accuracy, where “accuracy is the degree of conformity with a standard or measure of closeness to a value,” and precision was “the degree of refinement in the performance of an operation,” (Caltrans, 2015). For the purposes of analysis, photogrammetry standards from the USGS National Map Standards were used as well. According to the USGS orthoimagery requirements at a typical large-scale project are:

1. One-meter ground sample rate;
2. Bit depth of 8-bits; and
3. Current within three years of the map publication date.

The American Society for Photogrammetry and Remote Sensing (McGlone, Chris, 2013) categorically defines accuracy standards and definitions. The vertical and horizontal accuracies of any data are required to be at the 95% confidence level. Confidence level is the “percentage of

points within a dataset that are estimated to meet the stated accuracy; e.g., accuracy reported at the 95% confidence level means that 95% of the positions in the dataset will have an error with respect to true ground position that are equal to or smaller than the reported accuracy value,” (McGlone, Chris, 2013).

The Pix4D software generated a report that was used to determine the precision of the drone data. It was compared to the previously mentioned standards and then cross-referenced to the comparative data for precision/accuracy analysis.

Chapter 2 Related Work

This chapter briefly outlines the history of photogrammetry, and describes related work by presenting the core calculation methods of aerial photogrammetry and comparing them with semi-automated techniques used for aerial drone collections and the processing of the resulting spatial data.

2.1. Lineage

The sum of the careful observations of generations of humanity have evolved spatial analysis techniques to include precise, accurate, and accessible photogrammetry techniques in digital formats. Advancement is not without history.

Initiative, ingenuity, and sacrifice prevail throughout the historical annals of photogrammetry, and with notable characters. Gottfried Konecny described in his keynote address in 1985 four cyclical developments in photogrammetry through an approximate 50-year cycle (Konecny, 1985): (1) *Plane Table*; (2) *Analog*; (3) *Analytic*; and (4) *Digital*.

A fifth development could potentially be included as the craft blossoms. It is categorized by the readily available data easily accessible by the masses. It is: (5) *Information*. Information is historical. It serves to guide in establishing foundational work. The same processes used to determine precisions in older photogrammetry techniques are still viable usable calculations. Information is also innovative. It is the tools and materials needed for advancement. The growth of drone photogrammetry is served by readily available information.

2.1.2 Data Use

The end-product for the UAS drone data collection is cartographic presentation. The output is used in diverse ways, each situational by usage. Cartographic display includes (Konecny, 1985): (1) *Topography*; (2) *Location*; (3) *Base*; (4) *Volume*; and (5) *Flow*.

Topographical maps show natural and manmade features, specifically those that are representative of elevations and land formations. These maps use contour lines to show the earth's shape. Manmade features represented on these maps may include travel-ways, hydrological areas, survey control, and vegetation type (USGS, 2017). These types of maps are typically large scale (which is 1:10,000 to 1:25,000) if acquired from USGS yet can be as large as needed.

Inset maps are typically maps that are used to represent an overall location of an area. In the energy industry, inset maps are used to reference the larger representation. Similarly, orthorectified images are often used as background images for display of collected or created points and/or line-work in mapping. Drones can be utilized in the energy sector to further these mapping elements by providing up-to-date images. Flow maps and volume maps are different in that they provide rate information. In the energy sector they often relate to a watershed, and potentially focus on environmental and/or construction planning or remediation.

2.2. History

Notable inventions throughout history have led to the development of the current methods of retrieval, processing, and use of photogrammetric data. Leonardo da Vinci conceived of a device that enlarged images through glass. Albrecht Durer developed the mathematical

foundations of perspective geometry. It was further developed for use in photogrammetry by Rudolf Sturms through the relationship of projective geometry and photogrammetry. Daguerre continued the art by creating the photographic process of capturing images on a surface, called the Daguerreotype (Doyle, 1964).

Plane table photogrammetry, conceived by Aime Laussedat used the same principles as plane table surveying. Photographs were taken and placed by station according to resection and redrawn upon mapping paper. The age of analog photogrammetry heralded the use of stereoscopy and the airplane. Stereoscopy used dual images to create the perception of depth, while air flight by airplane made more collection with larger imaging at smaller scale possible. These bookmarks in history created the culmination of the combination of spatial analysis techniques into a singular niche, and historically cultivating the science of photogrammetry.

The digital age is considered the current age of photogrammetry. It is the technique for gathering digital imagery of objects to produce geometry with the information, including the application of metadata. Analysis of raster images is used for calculation, creating digital models, and for image backdrops for GIS visualization.

2.3. Relative Research

Surveying is the determination of positional data by collection or establishment. The surveying industry benefits from the advancement of collection methods. Still in its infancy, drone-use methods are an advancement in the capturing of necessary information including safer methods, and comparable results at better speeds. Drone make efficient use of time and resources, and establish an unmanned system capable of survey grade accuracy (Barry and

Coakley, n.d.). Topographic data in the survey field has been historically collected using time-consuming, on-the-ground methods with transit or level, and grew to include in recent history, Global Positioning Systems (DeGraeve and Smith, 2010).

Prior work using photogrammetry techniques are chronicled in the publication “Higher Surveying” from Breed, Hosmer, and Bone which was first published in 1908, and again in 1962, (Chapters 4 – 6). This publication provides a history of the process of aerial photography, including formulas that correlate the conventional calculation processes that were used to compare with middle-period and current methods. This work is accompanied by the article “The History of Photogrammetry” from the Center for Photogrammetric Training and penned by Gottfried Konecny. Writings that were used as reference for surveying terms and techniques were produced by Wolf and Ghilani’s “Elementary Surveying: An Introduction to Geomatics” and Singh, Artman, Taylor, and Brinton’s “Basic Surveying – Theory and Practice.” These works also serve to stress the importance of ground control parameters.

Current software practices include the processes and procedures for extrapolating data from UAS and techniques for creating accurate deliverables with the help of reference manuals (such as from Pix4D, ArcGIS, DJI Phantom 4, ArcGIS and AutoCAD). Additional writings of ongoing work include Karabork, Yildiz, Yilmaz, and Yakar’s “Investigation of Accuracy for Digital Elevation Models Generated with Different Methods in Photogrammetry,” Barry and Coakley’s “Accuracy of UAV Photogrammetry Compared with Network RTK GPS,” and Mitasova et al.’s “Raster based Analysis of Coastal Terrain Dynamics from Multitemporal LiDAR Data.” These works focus on the integration of accuracy, precision, and repeatability, which are the three elements of high order data collection and processing.

2.4. Precision and Accuracy Analysis Methods

There are no perfect measurements in surveying. All measurements consist, in some part, of errors. They are inherent in personnel, equipment, and the environment. Errors compiled in surveying data are adjusted through various methods of minimizing error propagation.

2.4.1 Formula

Repetition is the key to a successful analysis, specifically the ability of the data to be analyzed repeatedly with the same results. Historically, with technology advances, data collection from legacy and new systems, compared against each other, resulted in similar precision. According to “Aerial Photography and Image Interpretation” (Third Edition) by David P. Paine and James D. Kiser, scale and distance are measured, and are dependent relationally according to several factors: (1) the height of the instrument recording the photos; (2) the characteristics of the machine doing the recording; and (3) and environmental factors that produce image coordinates.

Interpretation is explanation. Interpretive geometry is the “process of recognizing and identifying objects and judging their significance through careful and systematic analysis” (Philpot, 2012). There are two main categories of photographs, terrestrial and aerial. Of these two interpretations, this photogrammetric effort focused on aerial. Aerial photographs are categorically vertical, oblique, or an infusion of both. Vertical photographs are perpendicular to the plane of capture, or most nearly so – with images slightly and advertently askew being referred to as tilted. Oblique image capture consist of images that are either low oblique – for example, recorded at a 30° angle off vertical which can be used to create 3D models – or, high

oblique – which are images that include a continuous field of view, that is – the horizon. All the test subject’s gimbal pitch angles were set to -90° , which indicated that the camera was facing straight down towards the ground, specifying that the pilot’s intentions were a flight pattern that was vertical, also known as nadir.

Statistical analysis of the horizontal and vertical accuracies was contrived using RMSE (root mean square error). Horizontal was assessed in the X, Y, and radial direction RMSE, while vertical was assessed using Z factors only.

The RMSE formula used is written:

$$1. \text{ RMSE} = \sqrt{\frac{1}{n} \sum_{i=1}^n (x_i(\text{map}) - x_i(\text{surveyed}))^2}; \text{ and}$$

$$2. \text{ Computation of Mean errors: } \bar{X} = \frac{1}{(n)} \sum_{i=1}^n X_i$$

where x_i is the i^{th} error in the specified direction, n is the number of checkpoints tested, and I is an integer ranging from 1 to n (McGlone, Chris, 2013).

RMSE report were generated from Pix4D, and were cross-referenced to the USGS data standards, according to ASPRS Accuracy Standards for Digital Geospatial Data taken from the online source (retrieved online September 2017).

Recall that the photo scale is determined by the formula $S = F/H-h$ (see Figure 2). The average height for flight for each of the test sites was 100 feet above ground level, and reiterating that the AGL was in this test was initiated by the Phantom 4 from a base height of 0.00 ft, and by machine specs concluding the focal length of the P4 as 24 mm (or, 0.07874 ft), and adjusted according to the GPS point 203 collected from the Asphalt test site zenith of 1226.729', and averaging the recorded LAS test points extrapolated from the file (Ohio State Plane South, NAD 83 average elevation 1228.558 ft to the third decimal significant figure).

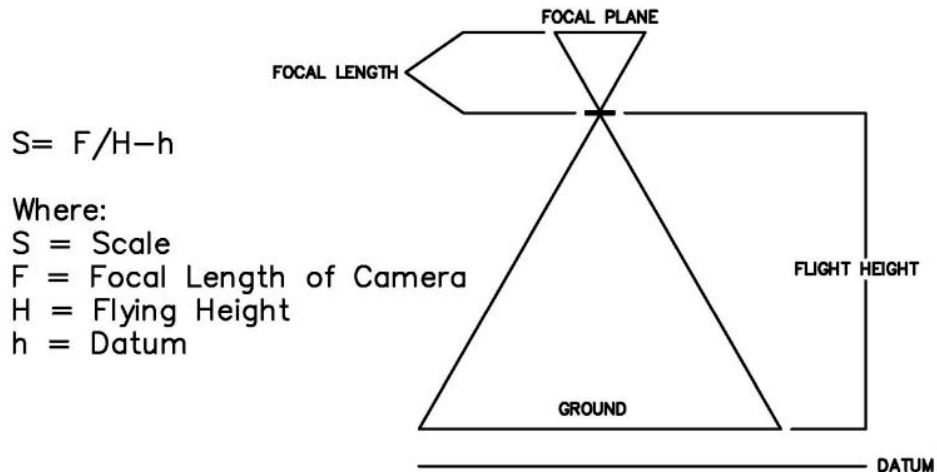


Figure 2 Scale and focal length interpretation.

For processing output to be accurate, the real focal length must be computed. Real focal length is:

$$Fr(\text{mm}) = (F35 * Sw) / 34.6$$

where $F35$ = focal length that corresponds to the 35mm equivalent, Fr = real focal length, and Sw = real sensor width, (Pix4D, 2017).

Photogrammetry solutions for accuracy and precision share similar characteristics to ground surveying. Precision and accuracy are based on a statistical analysis of triangular geometry, or the measurements and checks of angles in a triangle (Hallert, 1962). In such circumstances, the determination of angles is that the quality of measured data (shown in Figure 3)

$$N = a \sin z / \sin y$$

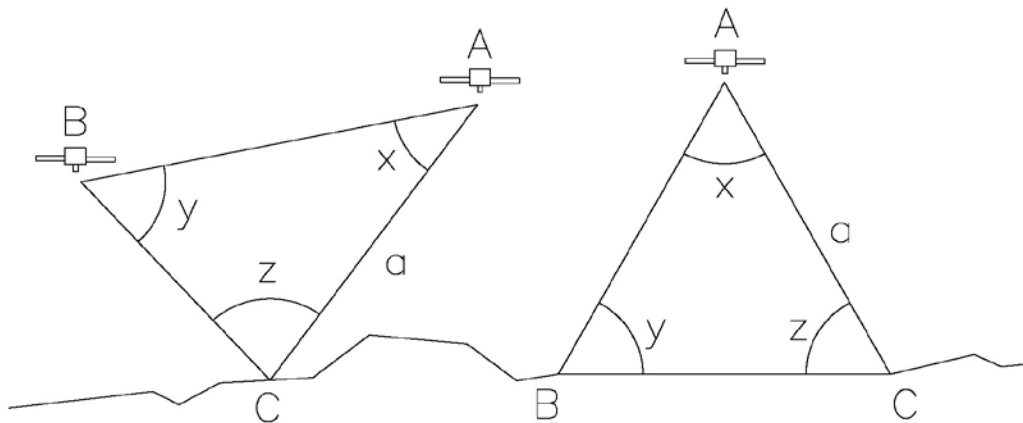


Figure 3 Trigonometry function of aerial triangulation

where a is the length or distance from aerial to ground, z is the interior angle of the triangulation, and y is the interior angle of the triangulation.

Furthermore, the geometric quality of N can be determined from the special law of error propagation. This law measures the effects of uncertainties in a list of variables. Quality

conforms with the replication of observations, and the results are a subsequent decrease of the average of the standard deviation. Adjustments are made accordingly, with least squares the preferred method. The least squares method is a best fit method, determined by the squared distance between data output and a regression line, and is recognized as using a solution that best approximates a value based on its relationship to other values in a general linear model. In basic terms, the sum of the measures divided by the number of measures is equal to the output. Therefore, taking the sum of the distances contrived from each calculation point in the photograph, creating best squares, and using that data in a standard deviation analysis systematically reduces error and increases theoretical precision and accuracy.

Chapter 3 Data and Methods

This chapter describes of the methods used to plan, gather, and process the drone collected data, which were then compared to Ohio OGRIP LiDAR as well as conventional survey data.

3.1. Comparative Data

LiDAR collected by the Ohio Department of Transportation was downloaded from the State's site. According to ODOT the provided LiDAR data met the requirements of positioning parameters, including vertical positioning using NAVD88 as orthometric height datum and Geoid model as GEOID12A. The coordinate system was area dependent. These projects were in the southern coordinate system of the state of Ohio. The map projection was Lambert Conformal Conic, the reference frame was NAD83 (2011), and the ellipsoid was GRS80.

Vertical error in LiDAR is ground dependent. Higher density data provides more accurate results. Because of LiDAR's ability to create dense datasets, highly vegetated areas are more likely to be recorded correctly because more points pass through the vegetation (McGlone, Chris, 2013). The State of Ohio certifies its data according to the ASPRS 2013 Positional Accuracy Standards as accurate and precise imagery and elevation data.

3.2. Pre-Flight Planning

An RPIC is often contracted to record data in an area they are unfamiliar with. A preview of the area is recommended for pre-flight planning purposes, and to avoid blind flying. In some

instances, a digital preview of the area is acceptable as opposed to an in-the-field assessment. Planning by opening popular online map applications such as Google or Bing Maps, inputting the central position of the proposed flight area, and planning the flight pattern and GSP positions will suffice. For most of the project sites surveyed, a preview of the area from the in-the-field perspective was required to determine flight path and ground control positioning as up-to-date imagery was unavailable.

The project's site pre-flight planning was more than looking at the area of flight, it was visualizing the spatial qualities of the area with intention. There were major considerations in the layout and patterning assessments in the pre-flight planning process. Ground control, instrument staging, route coverage planning, and safety precautions and assessments were among measured constructs. Updated software, including firmware, was a requirement as well. Out-of-date software could have caused fly-away, whereby the aircraft and control unit miscommunicate, and the unit can proceed to fly erroneously, causing loss of machine and data. The weather check is necessary to ensure that machinery is not water damaged, or data compromised due to reflectance from precipitation or photographic consistency is unbalanced due to windy conditions. Common standards when preparing for the flight are necessary to ensure that precision and accuracy standards are met when completing the aerial survey.

Ground control were geographically referenced control points set inside the perimeter of each site. They were used in the software in the processing phase as a geographically referenced point used in the calibration of the orthomosaic photo set. They helped "tie-down" the survey. Typically, software producers recommend a minimum of 3 or 4 GCP's per project, but the number is project site specific and large ranges in elevation characterize decisions as to number.

The number of different images that share the same GCP in each of them is important as well, because evenly placed GCSs help minimize error in scale and orientation, and redundancy calculates into accuracy and precision.

The flight patterns are important as well. Efficient overlay, according to Dr. Abdullah of Penn State University, is one that exhibits front and side overlap of 70% and 60% respectively (Penn State University, 2016). While DJI GSP flight is automated, including pattern parameters, the need to understand the reason the machine automated the pattern was important because in planning overlap, speed, and other parameters are user defined (refer to Figure 4).

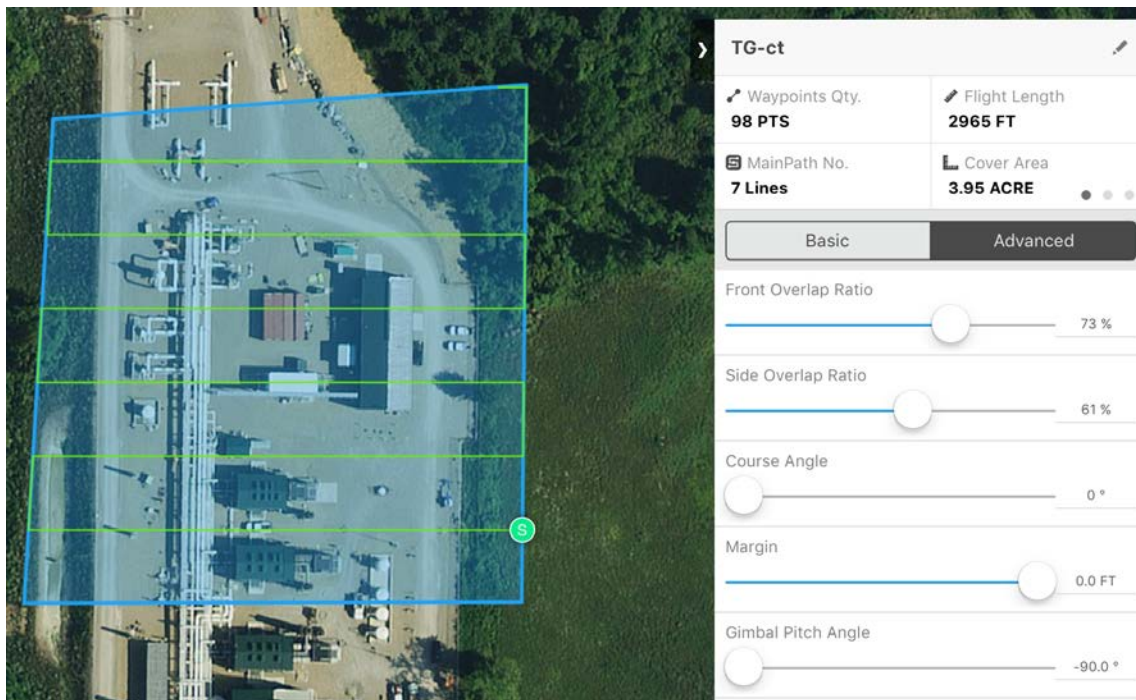


Figure 4 Flight parameters created in DJI GSP at the Tallgrass Site.

Setting up the flight pattern with fewer flight lines with less turns was the preferred option. Computing the lines themselves consisted of taking the single image ground coverage area and applying the following formula:

$$SP = IW \times (100 - SL) / 100$$

where SP is the distance between flight lines, IW is the image coverage area, and SL is sidelap.

After which, front lap is calculated:

$$FLN = (W/SP) + 1$$

where FLN is the flight line number, W is width, and SP is the distance between flight lines.

After the number of flight lines was numbered, the number of photos needed could be calculated.

Airbase (which is the distance between two photos) must be calculated using the formula:

$$B = IC(H) \times ((100 - EL) / 100)$$

where B is airbase, IC is image coverage, H is height, and EL is end lap. Then, the number of images per flight is calculated using the formula:

$$NI = (L/B) + 1$$

where NI is the number of images, L is length, and B is the airbase (Abdullah, 2016).

3.3. Project Flight

3.3.1 Flight Parameters

While each site had project specific parameters, similarities existed overall that aided in the formulation of patterning, including but not restricted to flight height, gimbal pitch, overlap and, overall coverage bounds. Adhering to this patterning, the Asphalt site, the Tallgrass, and the Dickinson sites each shared similar characteristics although each site had individual properties

that made them unique. Terrain features were different. The Asphalt site has a flat surface, but has ground features with steep elevation differences that constantly change. These being the piles of materials that were situated throughout the site. The Tallgrass site grounds have been permanently modified, and elevation changes were altered to include a gradual sloping pad that will not likely change in design in the future. The Dickinson site is an area with major contour changes that move into a draw to collect water, and is prone to change due to watershed processes. Yet, the drone could acquire data in these environments.

The drone calculated its flight height from an at-ground-level base and recorded it as 0.00 ft. This measurement system is based on wherever the unit records the base elevation as '0' and refers all other elevations higher or lower than the base as AGL or, Above Ground Level – which can incidentally include negative elevations – which should be a consideration in planning. The height of the instrument was then cross-referenced through the flight software (DJI GSP, in this case), and calibrated to real coordinate values. The DJI Phantom 4 drone that was used for these projects has an onboard GPS receiver. The receiver trilaterated the camera's position, which when relied upon alone to calculate geometry can accrue errors. In this case the iPad that housed the DJI GSP program and controlled the aerial flight was connected to a continually transmitting internet source routed through a Verizon MiFi, which created a third data-link with the machine in-air and geographic reference. This connection created a VRS referencing system that reduced flight errors to ± 1.2 inches vertical and/or horizontal error (Pix4D, 2017 and DJI, 2017).

The Phantom 4 Pro also uses the GPS/GLONASS satellite positioning system to measure location. Barometric sensors in the drone kept the machine at a level altitude when flying. The P4 barometer is a device that measures atmospheric pressure directly around the machine. The

machine also uses ultrasonic sensors. These sensors are designed to keep the machine from bumping or crashing into objects on all sides. In the case of the P4, the proprietary sensor mechanism is known as the Obstacle Sensing System. The steady altitude manufactured into the positioning of the P4 secured accuracy by eliminating flight height error influx into data acquisition.

While there are marked differences in the file formats used for UAS drone data when compared to LiDAR or traditional survey photogrammetry, the base methods in flight data collection have not changed. Flight patterns must be planned in a way that the area to be surveyed by the Remote Pilot in Charge (RPIC) is done so in a manner that captures more of the survey area than needed to ensure coverage. Over-coverage is desired. Photos are still categorically oblique or vertical.

Obliques are created by adjusting the degree of the camera opposite nadir which is considered perpendicular to the ground. Obliques are used in digital photogrammetry for 3D modeling. Vertical data is collected when the camera angle was nadir, or perpendicular to the ground. In some cases, oblique data is collected because of error in equipment or atmosphere. Bad weather conditions such as high winds or the pilot's inability to compensate for sharp turns or tight quarters can create unwanted parallax. This is referred to as drift. The same error can be reported when data is being attempted at oblique, and complications create unwanted results. Such errors can be a result of crab, which is the drifting of the craft off course of the pre-planned route.

Nadir is the flight characteristic where the plumb perspective of a single source in the orthomosaic, that being a single photograph, is a part of the whole “stitched” photograph. Photos that are vertical and provide a well-defined side and front overlap are preferred when creating the ortho, as image displacement can occur, and cause out of scale elements on post-processed data output, and shifts in perspective observed from various views creates inaccuracy.

When the UAS pilot photographs an area, the machine takes multiple photographs. These images must be arranged together to form a whole photo, called an orthomosaic (also referred to as ortho in this thesis). A UAS ortho is georeferenced by GPS collected through the quad-copter as well as through the collection of ground control points (GCPs). These GPS collected control points need to be situated throughout a test site in such a way as to help eliminate errors in calculation of position in the real world for vertical checks, that produced more accurate elevation data as well as tools for reducing or eliminating draping error. Flight path is an integral part in consistency in data collection, and consideration is given to include a high front (or, forward) overlap and sidelap percentages to ensure no area is left unphotographed.

3.3.2 Pix4D Correlations

The adoption of the previously defined parameters recommended by ASPRS were processed automatically through the Pix4D Desktop software, after quality assurances confirmed that the input information was recorded correctly. The GCP report correlated survey quality GNSS GPS data to the aerial data. Table 1 represents the singular accuracies for each control point, as well as the Mean, Sigma, and RMS Errors of the data collectively. The Projection Error column is the summation of the keypoint in each position relative to the GCP’s location. When

the keypoint's position is correlated to that of the GCP it creates a re-projection. The Projection Error is the sum of that error. The Verified/Marked column is created after the user marks the position of each GCP in photos. In this assessment, these positions were clarified by indicating this position in the file setup called the GCP editor.

Table 1 GCP report for error accuracy

| | | | |
|-----------------------|----------|----------|----------|
| Mean (ft) | 0.000000 | 0.000000 | 0.000000 |
| Sigma (ft) | 1.245790 | 1.632082 | 1.903370 |
| RMS Error (ft) | 1.245790 | 1.632082 | 1.903370 |

According to the Pix4D manual, the RMS error in the GCP error accuracy report “will take into account the systematic error,” and the “comparison of the RMS error and Sigma error indicates a systematic error. Of the 3 indicators, the RMS Error is the most representative of the error in the project since it (considers) both the mean error and the variance,” (Pix4D, 2017).

3.3.3 Scale and the Lens

Focal length and altitude affects each individual photograph, thereby potentially affecting the orthomosaic. Focal length is defined as the distance measured from the center of the lens to the focal point upon which the data is captured. It is relationally relevant to the ground data in the formula and defined in the drawing provided previously in Figure 2, page 15.

Photo scale is the ratio of the distance between two points on a photo, in relation to their position in real world. Map scale is the relationship of the distance between two points on a photo, correlative to position in the real world. For example, simple scale describes an object that

is one inch on a photo from another object, and the same two objects are one hundred feet in the real world then the scale is said to be 1:100. While photo scale and map scale are used similarly in that both represent accuracy, both have marked differences in derivation.

Choosing the correct camera to record photography is elemental in creating precise and accurate data. Detailed, aperture is the width of the opening of the shutter upon lens, and allows light into the camera and onto the image recording surface, and is important – as is the width of the lens itself (measured in millimeters) – in determining the focal capabilities of a camera. Typical narrow width apertures and slow shutter speeds are better at capturing wide areas with all the features in focus (the paradox being that a lens with a large aperture setting at high speed shutter settings will only be focused on elements in the center of the focus). Because of the focal length and aperture of the DJI Phantom 4's proprietary camera is built with a 94° field of view, and f/2.8 to f/11 autofocus at ± 1 meter, a focal length of 24 mm, and the ability to utilize a narrow aperture that compliments the focal length to capture successive full field of view images.

3.3.4 Tallgrass Site Flight Pattern

The Tallgrass Compressor site is home to several buildings, an expansive piping network, as well as mufflers and blow-off stacks. These provide a sharp contrast to ground data. The GCP layout procedure involved the placement of nine separate points in locations encircling the plant perimeter. It is notable to acknowledge that no points were placed in the middle area. The area is relatively flat. There are structures on the facility that prohibited extensive center-site placement. Figure 5 displays the GCP positional location throughout the site. The blue circle related to the

GCP's coordinate Z position while the green represents AGL. The green segments relate positional adjustments performed through P4D. Of the nine separate locations, each position was cross-referenced with 3 -5 of the in-flight photos using the software's GCP editor. All the points were recorded using high-precision GPS recording equipment from Trimble in the prescribed coordinate system. Ground control was set before the flight to ensure that the targets appear on the photos. There were eight GCP's on the site.

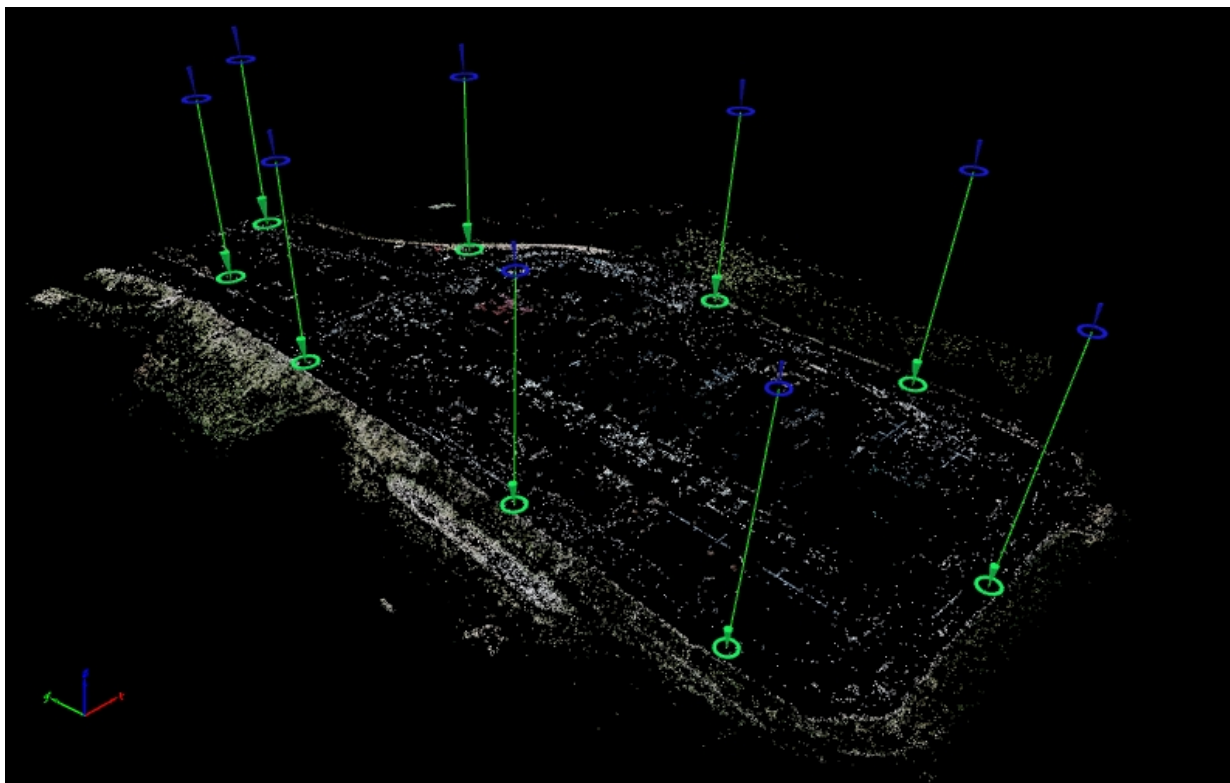


Figure 5 Tallgrass GCP placement location.

The Tallgrass site is the smallest, but with the most above-ground appurtenances of the test areas. The area is approximately 11.5 acres. Therefore, the RPIC identified that it was necessary to fly the site in four intervals from relative elevations in order to gather the best views

of the piping in the area. Another flight at a higher elevation was also completed in one overall pass to provide additional coverage for differential overlapping and referencing, as well as an approach to avoid unwanted parallax errors. The DJI Ground Station Pro software was utilized to perform the image capture. The flight parameters for one of the flight lines were indicated previously in Figure 4, page20.

The compressor plant was flown at two heights, 106.0 ft and 164.0 ft AGL. The images were compiled in one file and processed together. The purpose of multiple height flights is to retrieve ground detail from a low flight and top of structure detail from higher elevation. The resolution at 106.0 ft was 0.9 cm/px per meter, at 164 ft was 1.4 cm/px, and both elevations at the flight speed of 10.5 mph.

3.3.5 Asphalt Site Flight Pattern

The Asphalt site needed to create a cohesive overall product by noting that troubled areas needed more coverage This flight considered that by flying a pattern that was at least a ± 60 percent side-overlap and $\pm 70\%$ front-overlap within whichever current flight-path the program recorded, and rectified each separate segment of the flight, so that when combined to make a single unit, also adhered to similar patterns.

The flight speed was ± 10 mph to ensure that the machine's flight was smooth and parallel with the ground level, remembering that high winds can affect machine performance. The lower altitude AGL for the lower segment of the survey was ± 100 feet. The resolution of the imagery was 0.9 cm/px. This flight did not intend tilt (recalling that these are images derived from a camera angle $\pm 3^\circ$ to 30° from ground perpendicular) or oblique photography (images derived

from camera angle $\pm 35^\circ$ to 55° from ground perpendicular) into the data in order to use the output in stockpile volume calculations. The Asphalt site had nine GCP locations recorded throughout the site.

3.3.6 Dickinson Site Flight Pattern

The drone recorded photos of the lake with a 73% front overlap ratio and a 60% side overlap ratio. The gimbal pitch angle was at -90° , indicating nadir vertical to ground. Initial AGL (above ground level) was set constant at 103.4 feet with a camera resolution of 0.9 cm/px. The second AGL was set constant at 201.0 feet with a camera resolution of 1.7 cm/px. There was a difference in the AGL at the ± 200 feet constant of the Dickinson site with an AGL at 203.6 feet. The course speed for the missions were set at 10.5 mph. The Dickinson site had five GCP's placed throughout the location.

3.4. Data Extraction and Processing

While in the planning phase, the number of photographs that is required to be recorded is calculated to ensure sufficient information is available. The Phantom 4 Pro drone uses Micro Secure Digital removable storage. Smaller sites require less space onto which information needs to be stored, while testing, one to four-acre sites required at least a 32-gigabyte storage card. Larger projects require more storage, as in the case of the Tallgrass site. The amount of space required amounts to more than 50 gigabytes of space on two different 32-gigabyte cards, though it is possible to use larger storage sizes. Integral Memory boasts a 512 GB storage microSD card.

There are several methods that can be used to extract the data from the drone. The simplest and most widely-used method was to remove the Micro SD card and insert the card into

a laptop. The data recorded and stored on the card was transmitted into a folder for easy access from Pix4D.

Reconnaissance was performed by researching the tedious details of where ground control needed to be set, where to set the flight pattern and what type of data returns were needed for the site mapping types. After which, the RPIC's plan was put into action. The drone flew the preset pattern, collecting the necessary aerial info. The mission was a success. After which, the data was extracted and processed for use.

The image processing procedure in Pix4D was predominately automated after the system design values are assigned. The downloaded tif images were uploaded into Pix4D, the image properties were modified according to coordinate system, camera model, and accuracy. Processing options according to desired output use were chosen, meaning P4D allowed user processing input that included 3D maps and models, as well as multispectral and thermal mapping. GCP locations in the various corresponding images were correlated by choosing the same target in different photos so that the software could associate the images.

Pix4D class assignments were derived from machine-learned spectral analysis and compared to a set of previously tested materials via a proprietary machine algorithm. From these, elevation information was created (Becker, et al., 2017). This proprietary testing algorithm was used to compute classifications geometrically and by color into buildings, terrain, high vegetation, roads, human-made objects, or cars (Becker, et al., 2017), and into the last return, which is supposedly the ground return that is the desired class for best precision data extrapolation.

Destructive interferences in image capture and processing played a part in point classification. Sunlight – too much, or lack thereof – and ground objects with similar spectral properties could inadvertently be misclassified (e.g., vegetation, water, or man-made objects). Constructive interferences in the form of filters can be assimilated into the process – in initial capture, and into pre- or post- to overcome these obstacles. Lens filters and flight time-of-day planning choices reduced the chances of error in the field. Filters help reduce the effects of the Sun’s UV rays onto data. Choosing a time-of day to fly when the sun is overhead reduces shadow length, while early morning or evening casts more neutral light. Cloudy days produce even light. Histogram creation and interpretation methods aided in classifying point data.

3.5. Accuracies

The process of confirming accuracies and precisions was further met by extrapolating random elevation data from the LiDAR and drone refined DEM image and comparing the elevation data to GCP control points in the area. Comparison panels on random photos cross-referenced the Z of the nearby coordinates. The data was uploaded as a csv point file into Trimble Office and an inverse report was created and zenith data was compared from the GCP control point to each of the LAS test points.

The chart in Table 2 represents examples of the GCP’s that were chosen to compare the LAS data against. The columns defined are “OID” is the point number assigned to each GCP, chosen by the data collections person. The “Y”, “X”, and “Z” columns are representative of location. The “Description” and “Location” columns briefly describe attributes of each point, that being ground control target points specific to each test site.

Table 2 GCP comparison chart

| OID | Y | X | Z | DESCRIPTION | LOCATION |
|------------|------------|-------------|----------|--------------------|-----------------|
| 2 | 747715.55 | 2331115.96 | 1178.65 | TARGET | DICKINSON |
| 3 | 748059.06 | 2330924.42 | 1154.17 | TARGET | DICKINSON |
| 101 | 705680.958 | 2318898.293 | 1227.434 | TARGET | TALLGRASS |
| 104 | 705093.26 | 2319151.93 | 1231.191 | TARGET | TALLGRASS |
| 203 | 754124.29 | 2360173.614 | 1226.729 | TARGET | ASPHALT |
| 207 | 754451.195 | 2359674.005 | 1228.093 | TARGET | ASPHALT |

The observations reproduced in Table 3 shows a portion of the LAS data with the nearby point GCP 207 used as the comparative standard. The first column in the chart in Table 4 are the GCPs used in this ground-truthing. Column 2 is the LAS point from which the vertical inverse was derived. Columns 3 through 7 are the distance and bearing from which the GCP lays in relation to the inverse point. OGRIP data output points per meter being fewer in number than the UAS compiled data.

Table 3 Inversion report

| From | To | Geodetic Azimuth | Ellipsoid Distance | Grid Azimuth | Grid Distance (US survey foot) | Ground Distance (US survey foot) | Elevation (US survey foot) |
|-------------|-----------|-------------------------|---------------------------|---------------------|---------------------------------------|---|-----------------------------------|
| 207 | 1007022 | 69°06'14" | 0.552 | 69°06'14" | 0.552 | 0.552 | 0.004 |
| 207 | 622296 | 332°00'37" | 0.612 | 332°00'37" | 0.612 | 0.612 | 0.064 |
| 207 | 517380 | 43°29'52" | 1.43 | 43°29'52" | 1.43 | 1.43 | 0.977 |
| 207 | 1007122 | 204°03'05" | 0.459 | 204°03'05" | 0.459 | 0.459 | 0.012 |
| 207 | 517302 | 232°53'25" | 4.971 | 232°53'25" | 4.971 | 4.971 | 0.727 |
| 207 | 518614 | 348°10'10" | 9.175 | 348°10'10" | 9.175 | 9.175 | 1.007 |

Inversion in the surveying profession is the process by which a set of point coordinate values is measured against another set. This is relational. The measure is initiated from a common monument, and measured to variable instances, and by inverting a set of objects against a standard enables individuals to derive deviation. The inverse method used herein employed various points inverted to the known position of GCP 207 that determined vertical consistency. Trilinear interpolation was the fundamental basis of this coordinate inversion. It is like bilinear interpolation because it uses coordinate geometry to calculate grid distance and bearing differences, but also considers the zenith, or vertical differences in the calculation.

According to Mitasova et al. while confirming per-cell statistical analysis of LiDAR data, that higher point densities created terrain oversampling, yet not necessarily to the negative effect, but “provided excellent representation of sharp edges and breaklines,” which are primary datasets that topographical mapping relies on. Furthermore, the referenced research concluded that LiDAR data shifted due to terrain change. These conclusions, although based on coastal change are relatable findings in the energy industry’s pipeline services because the movement of the natural grade and terrain coverage influences topsoil characteristics.

Observations based on data from Table 4 which represents the points that were randomly chosen from the OGRIP LiDAR tiles. The “POINT_RECORD” column represents the assigned return point number in each tile. The intensity is the return strength collected from each point on the reflectivity of the object struck. Additionally, the reflectivity is the wavelength function determined by object composition, (Esri, 2017). The “CLASS_CODE” column represents the return classification code. In these cases, all returns were “2”, indicating “Ground” – also referred to as last return. The “X”, “Y”, and “Z” columns are the location data. The

“GPS_TIME” column represents the collection time of the LiDAR. The time was determined using OGRIP website information. The tiles for this project are from the 2014 OSIP data source (Ohio.gov, 2017).

Table 4 LiDAR report chart

| PNT RCRD | INTENSITY | NO RTRNS | CLASS CODE | X | Y | Z | GPS TIME | LAS REF |
|----------|-----------|----------|------------|-----------|-----------|---------|-----------|----------|
| 323663 | 157 | 1 | 2 | 2331118.5 | 747713.38 | 1179.2 | 60814.988 | s2330745 |
| 322767 | 173 | 1 | 2 | 2331111.3 | 747722.5 | 1178.77 | 60814.956 | s2330745 |
| 323664 | 171 | 1 | 2 | 2331109.9 | 747714.34 | 1180.2 | 60814.988 | s2330745 |
| 296348 | 61 | 1 | 2 | 2330926.2 | 748061.54 | 1149.19 | 60813.683 | s2330745 |
| 296347 | 144 | 1 | 2 | 2330917.8 | 748062.37 | 1149.71 | 60813.716 | s2330745 |
| 297177 | 80 | 1 | 2 | 2330924.9 | 748052.85 | 1150.5 | 60813.716 | s2330745 |
| 517380 | 158 | 1 | 2 | 2359675 | 754452.23 | 1229.07 | 343955.14 | s2355750 |
| 517302 | 204 | 1 | 2 | 2359670 | 754448.2 | 1228.82 | 343955.13 | s2355750 |
| 518614 | 82 | 1 | 2 | 2359672.1 | 754460.18 | 1229.1 | 343955.18 | s2355750 |
| 150418 | 128 | 1 | 2 | 2360174.4 | 754121.62 | 1226.14 | 341947.31 | s2355750 |
| 149344 | 180 | 1 | 2 | 2360177.9 | 754130.16 | 1226.17 | 341947.28 | s2355750 |
| 149343 | 195 | 1 | 2 | 2360170.2 | 754131.67 | 1226.65 | 341947.28 | s2355750 |
| 652271 | 207 | 1 | 2 | 2319150.1 | 705097.4 | 1229.95 | 236034.27 | s2315705 |
| 652272 | 180 | 1 | 2 | 2319160.1 | 705095.19 | 1230.15 | 236034.27 | s2315705 |
| 651957 | 189 | 1 | 2 | 2319148.4 | 705101.44 | 1230.2 | 236034.25 | s2315705 |
| 628767 | 212 | 1 | 2 | 2318899.7 | 705682.33 | 1219.49 | 236032.13 | s2315705 |
| 628766 | 209 | 1 | 2 | 2318891.1 | 705684.5 | 1220.63 | 236032.13 | s2315705 |
| 629042 | 183 | 1 | 2 | 2318900 | 705675.2 | 1220.54 | 236032.16 | s2315705 |

Image resolution per-pixel was a determining factor in precision assessment. The image resolution in digital photogrammetry is important, because the precision in scale is relationally determined based on the resolution of the image. The OGRIP data output is 6 in pixel resolution, with an 8-bit RGB rectified image producing a 2.5 ft DEM. In comparison, the data produced by the UAS and Pix4D was a 2 cm pixel resolution, 8 bit RGB image producing a ground sampling

distance (GSD) average of approximately ± 1 cm per meter (although 16 bit input/output is possible).

Scale was important in the assessment of accuracy. It was determined by calculation adhering to standard requirements. Spatial representation was indicative of user need. Client tailored mapping in the energy industry is commonly tailored to client requests and requirements. Knowing that the produced imagery is in digital format, and is represented in pixels, the pixels were analyzed to produce Ground Resolve Distance – which is the primary measure of spatial resolution, and are the smallest measurable distance on the image, (Campbell & Wynne, 2011). The pixels were dissected, and GRD resolution translated by the formula $GRD = H/(f)*(R)$ where GRD is the Ground Resolve Distance, H is the flying altitude above terrain, f is the focal length, and R is the system's resolution (Campbell and Wynne, 2011). This measure is an important interpretation of the purposing of the imagery.

Ground Sampling Distance is the “distance between two consecutive points on the ground (and) influences the accuracy and quality of the final results” in precision of the Pix 4D data output (Pix4D, 2017). This created a point cloud that was denser than the OGRIP LAS, with one testing sample a 20:1 UAS to OGRIP point ratio. Ground sampling distance is calculated:

$$Dw = (imW*GSD)/100$$

where Dw = distance covered on the ground per image (m) by width, imW = image width, and GSD = desired (required) Ground Sampling Distance (cm/px), (Pix4D, 2017).

Photo scale is used relationally with map scale to determine overall scale for comparative analysis. Map scale is defined as the scale of the photo divided by scale of the map equals the map distance divided by the photo distance, or $SP/SM = MD/PD$. This relationship was important in assessing accuracy comparisons, as all scales should be equivalent, as unequal outcome indicates error.

Drones provide visuals captured at hover, and equipped with the ability to rapidly store data. The collection methods are relative intrinsically to the data accuracy and precision. When techniques that are made provable are utilized according to outlined specifications, favorable results incur.

Chapter 4 Results

This chapter outlines the results and comparisons with USGS data that is certified by the ASPRS as precise and reliable information.

4.1. Results Analysis

Replicated and repeated measurements are different. Both are important in accuracy representation. Utilizing RMSE calculation and addressing elevations accuracy of the produced DEM, the RMS calculated differences between field elevation points and elevations that are obtained from points of DEM by interpolation produced consistent numbers. “The image correlation and the automatic derivation of a DEM can also be used as starting for the generation of digital orthophoto,” (Karabork, et al, 2004). Karabork iterates data matches by calculation and grid. Results are approximately the same (Karabork, et al, 2004). Results remind that replicated measurements are created in one place in one period, and repeated measurements are those that are taken at different time periods.

Furthermore, the standard deviation comparison with the data gathered and compiled in maps, agreed with the statistical analysis performed by the processing software and correlated with ASPRS standards. (It should be noted that the calculations were based on a testing area that was variable in nature, and the most desirable results were calculated in controlled environments, such as a perfectly flat area with minimal environmental interferences, such as high winds, barometric flux, or high solar reflectance).

The data in Table 5 shows the typical absolute camera position and orientation uncertainties of the Dickinson Site. This excerpt of the report was typical to other reports generated on the other test site projects. It is used to verify that the mean error (average error in each direction – X, Y, Z), and sigma (standard deviation of the error in each direction – X, Y, Z) were of acceptable return. X Y Z are the cartesian equivalent of longitude, latitude, and zenith of a measurement, respectfully. Omega is the rotation of the output around the X-axis. Phi is the rotation around the Y-axis. Kappa represents the rotation around the Z-axis. Differences in data that result in unusable errors are determined by the output. In this case, the averages resulted in an overall Sigma error of less than a tenth in the X and Y quadrants and about three inches error in the overall vertical measurements in Z.

Table 5 Absolute camera and deviation uncertainties

| | X (ft) | Y (ft) | Z (ft) | Omega (degree) | Phi (degree) | Kappa (degree) |
|--------------|---------------|---------------|---------------|-----------------------|---------------------|-----------------------|
| Mean | 0.23 | 0.22 | 0.48 | 0.043 | 0.052 | 0.015 |
| Sigma | 0.06 | 0.06 | 0.14 | 0.006 | 0.014 | 0.006 |

Furthermore, according to Mitsova, et al. that, application dependent, "...various functions can be used, from simple statistics, such as mean, median, mode, minimum, maximum, standard deviation, and diversity, to more complex relationships, such as linear regression slope, offset, and coefficient of determination, computed for each cell. The temporal aspect of terrain evolution can be analyzed using a map that represents the time when the given cell was at its lowest elevation and a map representing the time when each cell was at its highest elevation,"

(Mitasova, et al, 2009). For the purposes of this study, simple statistical observations calculating the mean averages of a set of observed points as inversed to a GCP were administered.

The results in Table 6 were representative of the overall accuracy of the geolocation of the photographs. The numbers verify that 99.38% of photographs used were within ± 1 foot, and all were within ± 2 and 3 feet, verifying that the software verified data results in high-order data accuracy.

Table 6 Relative geolocation variance report for the Asphalt site

| Relative Geolocation Error | Images X [%] | Images Y [%] | Images Z [%] |
|---|--------------|--------------|---------------------|
| [-1.00, 1.00] | 99.38 | 100.00 | 99.07 |
| [-2.00, 2.00] | 100.00 | 100.00 | 100.00 |
| [-3.00, 3.00] | 100.00 | 100.00 | 100.00 |
| Mean of Geolocation Accuracy (ft) | 5.00 | 5.00 | 10.00 |
| Sigma of Geolocation Accuracy (ft) | 0.00 | 0.00 | 0.00 |
| Geolocation Orientational Variance | | | RMS [degree] |
| Omega | | | 0.96 |
| Phi | | | 0.58 |
| Kappa | | | 5.27 |

Additionally, Mitasova, et al. iterates the importance of GPS accuracy implementation in precision discovery, as in the case of this report. The GCP GPS data, when used as reference for reporting. They write that “the accuracy of the RTK GPS survey along the (survey area) was sufficiently higher than the published accuracy of the LiDAR surveys...making the RTK GPS data suitable for assessment of the actual LiDAR data accuracy,” (Mitasova et al, 2009). As mentioned previously, similar observations were created when comparing LAS points derived from the drone by inversion to the GCP and the LAS derived from OGRIP.

4.2. Individual Site Results

4.2.1 Asphalt Site

The Asphalt site data processing resulted in an average ground sampling distance of 0.82 cm/0.32 in in the covered 14.8164 acres. Recall that ground sampling distance is the linear distance between two measured pixels on the ground. The larger the GSD, the less resolution an image or data has (Pix4D, 2017). There were 9,921 calibrated 2D matches per image with 10 GCPs with a mean RMS error of 0.051 ft. The absolute camera position and orientation uncertainties mean (average) in the XYZ were 0.029, 0.026, and 0.114, respectively. The mean omega, phi, and kappa – (3D accuracy) were 0.006, 0.009, and 0.003 respectively. The absolute camera position and orientation uncertainties sigma (standard deviation) in the XYZ were 0.007, 0.007, and 0.033, respectively. The sigma omega, phi, and kappa – (3D accuracy) were 0.002, 0.003, and 0.001, respectively.

There were 5,059,956 2D keypoint observations in the bundle block adjustment, with a mean average of 30320 keypoints per image, a mean projection error of 0.155, and 9,921 matched keypoints per image, indicating the number of matching points that the software can use to assess 3D information in each image.

Ground control point accuracy in the XY/Z parameters were 0.020/0.020. The mean error of the X was 0.001849, the sigma of the X error was 0.065245, and the RMSE of the X was 0.065271. The mean error of the Y was -0.003252, the sigma of the Y error was 0.066500, and the RMSE of the Y was 0.066580. The mean error of the Z was 0.006644, the sigma of the Z error was 0.023135, and the RMSE of the Z was 0.024070.

Random samples taken from the LAS data at the Asphalt site derived around GCP point 208 indicates that there is an Z mean of 1230.578 ft elevation with average deviation of the Z mean of 0.086667. In contrast, there is a vertical difference of 2.2170 between the GCP and OGRIP LiDAR data (reference Table 7).

Table 7 Asphalt random samples

| OID | Y | X | Z | DESCRIPTION |
|---------|------------|-------------|-------------|-------------|
| 208 | 754285.301 | 2359710.95 | 1230.703 | TARGET |
| 1544815 | 754285.376 | 2359710.805 | 1230.405 | LAS |
| 1206500 | 754285.264 | 2359711.104 | 1230.72 | LAS |
| 805391 | 754284.911 | 2359710.797 | 1230.61 | LAS |
| 496606 | 754285.87 | 2359709.06 | 1232.92 | LIDAR |
| | | Z Mean: | 1230.578333 | |
| | | Z SD: | 0.08666667 | |

4.2.2 Dickinson Site

The Dickinson site data processing resulted in an average ground sampling distance of 1.03 cm/0.4 in in the covered 13.5705 acres. There was a median of 5,876 calibrated 2D matches per image, with five GCPs and a mean RMSE of 0.082 ft. The absolute camera position and orientation uncertainties mean (average) in the XYZ were 0.068, 0.063, and 0.121, respectively. The mean omega, phi, and kappa – (3D accuracy) were 0.011, 0.015, and 0.004, respectively. The absolute camera position and orientation uncertainties sigma (standard deviation) in the

XYZ were 0.019, 0.018, and 0.037, respectively. The sigma omega, phi, and kappa – (3D accuracy) were 0.003, 0.004, and 0.002, respectively. There were 2,222,381 2D keypoint observations in the bundle block adjustment, with a mean average of 46,624 keypoints per image, a mean projection error (pixels) of 0.158, and 5,876 matched keypoints per image.

Ground control point accuracy in the XY/Z parameters were 0.020/0.020. The mean error of the X was 0.011172, the sigma of the X error was 0.075243, and the RMSE of the X was 0.076068. The mean error of the Y was -0.013287, the sigma of the Y error was 0.072070, and the RMSE of the Y was 0.073284. The mean error of the Z was 0.015463, the sigma of the Z error was 0.100630, and the RMSE of the Z was 0.101811.

Random samples taken from the LAS data at the Dickinson site derived around GCP point 3 indicates that there is a Z mean of 1154.15 ft elevation with an average deviation of the Z mean of 0.0220 (reference Table 8).

Table 8 Dickinson random samples

| OID | Y | X | Z | DESCRIPTION |
|--------|------------|-------------|----------|-------------|
| 3 | 748059.064 | 2330924.416 | 1154.171 | TARGET |
| 483030 | 748058.894 | 2330923.95 | 1154.181 | LAS |
| 94555 | 748059.542 | 2330924.655 | 1154.106 | LAS |
| 32067 | 748058.792 | 2330925.213 | 1154.163 | LAS |
| 296348 | 748061.53 | 2330926.07 | 1149.19 | LIDAR |
| | | Z Mean: | 1154.15 | |
| | | Z SD: | 0.022 | |

4.2.3 Tallgrass Site

The Tallgrass site data processing resulted in an average ground sampling distance of 1.86 cm/0.73 in in the covered 7.6879 acres. There were 3,920 calibrated matches per image with nine GCPs with a mean RMSE of 0.009 ft. The absolute camera position and orientation uncertainties mean (average) in the XYZ were 0.387, 0.481, and 5.964, respectively. The mean omega, phi, and kappa – (3D accuracy) were 0.043, 0.049, and 0.009, respectively. The absolute camera position and orientation uncertainties sigma (standard deviation) in the XYZ were 0.064, 0.021, and 0.106, respectively. The sigma omega, phi, and kappa – (3D accuracy) were 0.007, 0.020, and 0.006, respectively. There were 32,748 2D keypoint observations in the bundle block adjustment, with a mean average of 3,920 keypoints per image, and 648 matched keypoints per image.

Random samples taken from the LAS data at the Tallgrass site (A) derived around GCP point 109 indicates that there is a Z mean of 1225.172667 ft elevation with an average deviation of 0.055667. (reference Table 9).

Table 9 Tallgrass random samples (A)

| OID | Y | X | Z | DESCRIPTION |
|------|------------|-------------|-------------|-------------|
| 109 | 705265.124 | 2318852.466 | 1225.284 | TARGET |
| 3326 | 705265.754 | 2318853.633 | 1225.154 | LAS |
| 980 | 705258.406 | 2318853.791 | 1225.08 | LAS |
| | | Z Mean: | 1225.172667 | |
| | | Z SD: | 0.05566667 | |

Ground control point accuracy in the XY/Z parameters were 0.020/0.020. The mean error of the X was -0.000821, the sigma of the X error was 0.004411, and the RMSE of the X was 0.004487. The mean error of the Y was -0.002522, the sigma of the Y error was 0.006841, and the RMSE of the Y was 0.007291. The mean error of the Z was 0.007173, the sigma of the Z error was 0.017892, and the RMSE of the Z was 0.019276.

Random samples taken from the LAS data at the Tallgrass site (B) derived around GCP point 3 indicates that there is a Z mean of 1154.15 ft elevation with an average deviation of the Z mean of 0.093. Visual assessment was performed by contriving building position cross-referenced with as-built (reference Table 10)

Table 10 Tallgrass random samples (B)

| OID | Y | X | Z | DESCRIPTION |
|------------|-------------|-------------|----------|--------------------|
| 106 | 2318991.437 | 704757.168 | 1228.376 | TARGET |
| 10362 | 704756.878 | 2318994.019 | 1228.627 | LAS |
| 5521 | 704762.027 | 2318987.276 | 1228.32 | LAS |
| | | Z Mean: | 1228.441 | |
| | | Z SD: | 0.093 | |

4.3. Confidence Levels

The hypothesis confidence level was reportedly a $\pm 98\%$. Samples derived from the LAS and compared to GCP, as well as data tested in Pix4D's statistical computations agreed with this conclusion. Observed samples tested randomly with deviation calculations as noted in Table 7

appeared to be similarly accurate. A rasterized vector derived from the DEM and the subsequent histogram of the vertical data derived from Terrset also agreed with the data output in Pix4D, and as observed by contour line generation visual comparison.

Table 11 Deviation report

| POINT RECORD | Y | X | Z | PARENT LOCATION A Sample |
|---|-------------------------------|-------------|------------|---------------------------------|
| 150419 | 754123.146 | 2360166.87 | 1226.33 | s2360750 |
| 844333 | 754123.949 | 2360165.654 | 1226.517 | Asphalt Results Tracks 2 |
| 817224 | 754122.973 | 2360168.931 | 1226.495 | Asphalt Results Tracks 2 |
| 150435 | 754120.303 | 2360165.437 | 1226.56 | s2360750 |
| | <i>Average of the samples</i> | | 1226.4755 | |
| <i>Average deviation of the samples</i> | | | | 0.07275 |
| POINT RECORD | Y | X | Z | PARENT LOCATION B Sample |
| 61994 | 747760.881 | 2330755.766 | 1212.1 | s2330745 |
| 701060 | 747760.291 | 2330753.544 | 1212.553 | Dickinson Results Tracks 2 |
| 701164 | 747763.225 | 2330753.822 | 1212.487 | Dickinson Results Tracks 2 |
| 701252 | 747763.225 | 2330758.613 | 1212.067 | Dickinson Results Tracks 2 |
| | <i>Average of the samples</i> | | 1212.30175 | |
| <i>Average deviation of the samples</i> | | | | 0.21825 |

Considerations were taken to avoid a null hypothesis by avoiding contamination of the test data. The current test statistics rejected the null hypothesis, but more random sampling was needed to conclude irrefutable results. The implications derived from the analysis of the

information are that the random sampling of the drone LAS data was a part of the expected population. The conclusion of this report is that Pix4D can create a point cloud that is similar in vertical output as LiDAR, and meets or exceeds ASPRS confidence levels.

The OGRIP data download was expected to, and did meet and/or exceed horizontal and vertical accuracy standards. Horizontal accuracies for maps represented in a scale of larger than 1:20,000 specify they are not allowed to have more than 10% of well-defined points with an error of more than 1/30 inch as measured on the published scale. Maps with smaller scales than 1:20,000 are allowed 1/50 inch (Caltrans, 2012). Similarly, vertical accuracies require no more than 10% of elevations can be in error by more than one-half of a contour interval, (Caltrans, 2012). LiDAR downloaded from Ohio's data vault met the parameters of page A9 of the ASPRS report of Photogrammetric Engineering and Remote Sensing, more specifically the Annex C, Accuracy Testing and Reporting Guidelines on page A18 (ASPRS, 2015). The report continues by describing that errors in LiDAR are a result of GNSS positional errors, INS (inertial navigation systems) angular error, and flying altitude. Table 4 is the expected error in horizontal data (RMSE) in terms of altitude (ASPRS, 2015), and can be scaled relatively into any project's parameters. Each of the testing areas produced the same results, that being contour data produced from both sets of data and measured between each other are consistent in elevation one to the other, as well as vertical point data being within the ASPRS standards using a 95% confidence level.

Additional, referring to Table 6, page 36 we infer calculations derived from column four, six, and seven shows that 67% of the points were within two feet of the GCP test point, whereas the other $\pm 33\%$ were between ± 5 to 10 feet. It is noted that this is typical when comparing the

two LAS datasets, as the data derived from the drone proved far denser in point composition than the OGRIP LAS data. This is due to the OGRIP data output points per meter being fewer in number than the UAS compiled data. Visual comparison of the one square meter testing further confirmed compared point density.

It was pertinent to keep in consideration in the testing parameters that systematic errors were unavoidable, but typically follow fixed predictable patterns. The specific values that were accepted as accurate from the calculations varied from project to project, but remembering that ASPRS designated that there be less than a 25% error between the mean output and specified RMSE. While Pix4D calculates the accuracy with automation, it is important to understand the process by which errors occur so that errors can be detected and corrected. The horizontal accuracy that was compared by planimetric coordinates (specifically, OH83-NF, which is Ohio South State Plane coordinates on the NAD 83 datum grid), and additional vertical datum from USGS monumentation and/or previously verified monumentation. Low-confidence areas were also used in consideration, and ASPRS digital data guidelines that indicate these areas be developed into polygons and results and reasonings explained in the metadata (ASPRS, 2015).

Chapter 5 Discussion and Conclusions

The FAA's change in regulation to allow the acquisition of UAS drone commercial licensure has yet to reach its anniversary date to which its initial class must apply for license reissue. The commercial drone data collection industry is still in its infancy, but the ability of the innate perception of spatial data planning, the visual conception of a project rigorously processed competently through credible resources, and the material cross-referenced against dependable sources can create desirable, usable data output. This section summarizes the data collected, processed, and how the subsequent results affect the scope of the project.

5.1. SWOT (Strengths Weaknesses Opportunities Threats) Analysis

The SWOT for UAS drone technology is noticeably intertwined. The recently changed FAA regulations created rapid advancement in the use of these systems as a mode of data collection but not without consequences.

5.1.1 Strengths

There are several key strengths to the use of UAS drones to capture aerial images. The initial prospect is described in this thesis, that being the ability of the system to create reliable data that can be used in a variety of mapping and analysis projects. The accurate point clouds derived from drones can depict topographical data used for construction planning and monitoring of sites, equipment and appurtenances. The imagery derived can be used as visual aids in planning as well as in situations where recent photos are a requirement, as in the case of

ALTA/NSPS land surveys, where up-to-date imagery is attached to finalized plats for visual proofing in documentation.

The Phantom 4 machine and its controlling software is user-friendly, and takes a minimum amount of training to acquire data on a mission. The software can be learned in minutes. The drone comes equipped with a pre-set amateur parameter in the form of collision avoidance settings, that when followed correctly keep an inexperienced user from colliding with foreign objects

The data can be used in a variety of software. There are multiple outputs of the processed data. The tif images can be used in programs like Terrset or QGIS and stitched together in a mosaic manually and the topographical information analyzed. Other programs, such as Pix4D used in this project, have multiple output formats including the DSM and DTM formats, georeferenced Orthomosaic, contours, point cloud, mesh, volume calculations, and quality reports.

5.1.2 Weaknesses

One of the major weaknesses found using the system is an adverse result from the UAS drone's strength in the form of its ease of use. The system's focus on beginning RPICs in a quickly growing industry opens doors that possibly should not be opened, which can result in the proverbial Pandora's Box. Prospective users who have little or no training in surveying or spatial analysis collect data without knowing the accuracy or inaccuracy of the output data. The open-door policy of the new technology fosters growth, as well as error. Additionally, the data output has not been considered 'certifiable' by many in the surveying profession.

The quality of the Phantom 4 Pro is at a the low-end of professional grade, and while it works well for academic purposes and less experienced RPICs the machine's limited capabilities are obvious to experienced users. The device cannot change camera types because the gimbal is not interchangeable. The payload is low-weight, so attaching other types of sensors or mechanisms to it were not recommended by the manufacturer at the time of this research.

5.1.3 Opportunities

There are many opportunities, including the production of the aforementioned topographical data and photographic imagery, that are available. There is also the UAS ability to perform visual inspection. The photography from this data type can be also be extracted with Pix4D and used in the creation of 3D imagery. The technology houses formats that include the sciences of thermal and magnetic sensing collection and inspection, which are all applicable formats used in the energy industry.

5.1.4 Threats

Deviation is the threat to the energy industry. Deviating from sound collection methods threatens the accuracy of data. Deviating from proven processing techniques may produce unusable output. Deviating from FAA rules and regulations makes for unregulated flying conditions that may be unsafe and counterproductive.

Users who fail to adhere to the fundamental techniques of spatial data collection and processing may create erroneous data output, threatening the science's credibility. If enough bad data is produced, then the possibility of growing distrust in the industry is greater and will

threaten its growth. Additionally, failure to comply with FAA regulations will create more regulations, stifling growth. Adversely and consequently, the FAA's inability to monitor the growth rate of new users can introduce too many new users into the field, the influx of new users could potentially cause the market value to drop.

5.2. Sources of Error and Problems

The drone and machine software processes proved reliable in most instances when firmware was updated, and maintenance kept regular. There were issues that were encountered recording and processing these three sites of the project. Sources of human or machine processing and collections error include: unforeseen or uncontrollable, natural complications – including weather forecast planning, machine and software failures, collection and processing error.

Windy conditions caused the machine to move erratically and work harder to maintain its calculated course. This caused the battery life to diminish quicker than in normal conditions. Low battery conditions can lead to “fly-away.” This error is one where the machine's programming erroneously searches out its last known landing position, and if it is not in a close location (because of human error in shortsighted planning), then the machine will search for that initial take-off position until it drops out of the sky. This situation is funny to think about in hindsight, but when the predicament occurs and the RPIC realizes that the last ‘Home’ base is 40 miles away in the next city it becomes a serious problem. These cases are prevalent in corridor surveys where miles of straight-line collections are made. Wind also caused tilt in the machine. This resulted in the gimbal to over-compensate to capture a flat photograph. While the machine is calibrated to compensate for this error, the RPIC must maintain the calibration manually. By

this human error is introduced. Likewise, during overly gusty conditions, the gimbal often cannot compensate quickly enough to capture a nadir photograph.

Machine failure can complicate the data collection process when utilizing the UAS drone. The Phantom 4 requires regular updates to its software and firmware. Failure to do so can lead to non-flight, crashes, fly-away, non-collection, and miss-collection. DJI recommends updating machine and software fixes available for the RPIC to prevent or correct known issues (DJI, 2017).

Ground Control Points were placed specifically in logical positions and used to “tie-down” the area’s XYZ. Errors in GCP surveys typically include input of incorrect datum systems. State Plane systems can include similar datum projections that can produce results that can be missed in the processing segment. For example, while ArcGIS is an excellent software to integrate various coordinate systems it cannot compensate for the observed four-foot vertical error that accrues processing in State Plane Ohio South HARN. Whilst the GCPs were recorded in State Plane Ohio South NAD 83, an incorrect categorization of projection would have yielded erroneous positions. Error produced while processing in Pix4D include misnaming GCPs and choosing the wrong GCP representation in the GCP/MTP Monitor. Typically, Pix4D compensated for this error, but made difficult efforts in ground-truthing.

5.3. Future Improvements

Future improvements include suggestions in machine and software, and technique updates. The technology that powers the machines will continue to improve. In the process of collecting diversified data, more expensive equipment is a requirement. Octocopters (eight rotor

machines) are more stable than the quadcopter used in this research. Additionally, higher resolution cameras produce more detailed images and better end-results.

Another advancement that can impact future improvements are the use of underground magnetic location, used for locating underground metallic structures such as abandoned well locations. One such device is the Fluxgate Magnetometer described in detail by Douglas G. Macharet, et al. 2016 and used to search for ferromagnetic materials underground. The need for UAS drones is evident by the parameters required for this sensing technique to perform accurate data collection. It needs: (1) *Precise North Oriented Coverage*; (2) *Point Separation Flight Planning*; (3) *AGL Control*; (4) *Hover* (Macharet, Douglas. et al., 2016).

Successful testing of underground locating of ferrous materials for mining purposes translates into the availability of the same technology as a crossover into the energy industry in the form of aerial locating of abandoned locations, and creating the possibility of modifying the receiver to focus signal reception based on sound wave detection that is particular to underground considerations. These sensors can be used to detect anomalies that exceed set ranges, and are safer for personnel by keeping them at acceptable distances from problem areas. These technologies presently exist, are growing, and will continue to grow into normal techniques for use in the energy sector. Finally, the possibility of writing python script that is able to extrapolate random samples from two or more LAS datasets and create statistical output based on given parameters will aid in the assimilation of random samples in LAS testing.

What should be said about drones? Is the current preoccupation with them because they are a cool toy? They are, indeed. But they are more than just a plaything atop a child's shelf left

to collect dust after the luster has gone. They are a tool that has now and in the future helped mold an industry to become more profitable economically and ergonomically. The tool is able to work in the energy industry by being able to provide safety to field personnel by allowing surveys of a wider area with precision and accurate data returns.

References

- ASPRS *Accuracy Standards for Digital Geospatial Data*. Current report to date, March 2015. Retrieved September 2017 from http://c.ymcdn.com/sites/www.mapps.org/resource/collection/DC6E171F-93D8-41FD-AF6E-AEDBB829867A/December_HLA_v3.pdf
- Band, Lawrence E. *Topographic Partition of Watersheds with Digital Elevation Models*. Water Resources Research. Vol. 22, No. 1. January 1986.
- Barry, Paudie., and Coakley, Ross. *Accuracy of UAV Photogrammetry Compared with Network RTK GPS*. Baseline Surveys, Ltd. n.d.
- Becker, C., Hani, N., Rosinskaya, E., d'Angelo, E., and Strecha, C. *Classification of Aerial Photogrammetric 3D Point Clouds*. Pix4D. May 2017.
- Bolstad, Paul. *GIS Fundamentals: A First Text on Geographic Information Systems*. 4th Ed. 2012.
- Breed, Charles, Hosmer, George, and Bone, Alexander. *Higher Surveying: Principles and Practice of Surveying, Volume II*. Massachusetts Institute of Technology. 8th Edition. 1962.
- Caltrans. Survey Manual – Chapter 5. California Department of Transportation. 2015. Retrieved September 2017: http://www.dot.ca.gov/hq/row/landsurveys/SurveysManual/05_Surveys.pdf
- Campbell, James B. & Wynne, Randolph H. *Introduction to Remote Sensing*. 5th Ed. The Guilford Press. 2011.

- Carrara, Alberto, Bitelli, Gabriele, and Carla, Roberto. *Comparison of Techniques for Generating Digital Terrain Models from Contour Lines*. International Journal of Geographical Information Science. Vol. 11, No. 5. 1997.
- Cho, Yeonmin *Lost in Debate: The Safety of Domestic Aircraft Systems*. Towson University. Journal of Strategic Security. 2014.
- Colomina, Ismael., Molina, Pere. *Unmanned Aerial Systems for Photogrammetry and Remote Sensing: A Review*. ISPRS Journal of Photogrammetry and Remote Sensing. 2013.
- DJI Phantom 4. *User Manual*. Version 1.0. 2016.
- Doyle, Fredrick. “*The Historical Development of Analytical Photogrammetry*”, Photogrammetric Engineering, 1964.
- Eastman, Ronald J. *TerrSet: Geospatial Monitoring and Modeling System*. Clark Labs. 2016.
- Fabris, Massimo and Pesci, Arianna. *Automated DEM Extraction in Digital Aerial Photogrammetry: Precisions and Validation for Mass Movement Monitoring*. ANNALS OF GEOPHYSICS, VOL. 48, N. 6, December. Dipartimento di Fisica, Settore Geofisica, Università degli Studi di Bologna, Italy. Istituto Nazionale di Geofisica e Vulcanologia, Sede di Bologna, Italy. 2005.
- Federal Aviation Administration. *Summary of Small Unmanned Aircraft Rule, Part 107*. 2016.

- Fonstad, Mark A., Dietrich, James T., Courville, Brittany C., Jensen, Jennifer L., and Carbonneau, Patricia E. *Topographic Structure from Motion: A new Development in Photogrammetric Measurement*. Earth Surface Processed and Landforms. 2012.
- Fuhong He, TaoWang, Lijuan Gu, Tao Li, Weiguo Jiang, and Hongbo Shao. *An Integrated Use of Topography with RSI in Gully Mapping, Shandong Peninsula, China*. 2014.
- De Graeve, Jan and Smith, Jim. *The History of Surveying*. International Federation of Surveyors. International Institution for the History of Surveying and Measurement FIG Permanent Institution. 2010.
- Jenson, Susan. and Domingue, Julia. *Extracting Topographic Structure from Digital Elevation Data for Geographic Information System Analysis*. Photogrammetric Engineering and Remote Sensing, Vol. 54, No. 11. 1988.
- Konecny, Gottfried. "The International Society for Photogrammetry and Remote Sensing - 75 Years Old, or 75 Years Young", Keynote Address, Photogrammetric Engineering and Remote Sensing, 51(7), pp 919-933. 1995.
- Hallert, Bertil. *Accuracy and Precision in Photogrammetry*. Photogrammetric Engineering. 1962.
- Mancini, Francesco, Dubbini, Marco, Gattelli, Mario, Stecchi, Francesco, Fabbri, Stefano, and Gabbianelli, Giovanni. *Using Unmanned Aerial Vehicles (UAV) for High-Resolution Reconstruction of Topography: The Structure from Motion Approach on Coastal Environments*. 2013.
- McGlone, Chris. ASPRS. *Manual of Photogrammetry*. 6th Edition. 2013.

- Mitasova, Helena, Overton, Margery F., Recalde, Juan Jose, Bernstein, David J., and Freeman, Christopher W. *Raster-Based Analysis of Coastal Terrain Dynamics from Multitemporal LiDAR Data*. Journal of Coastal Research. Volume 25. 2009
- M.R. Rifas Ahamed. *Historical Development of Photogrammetry*. Faculty of Geomatics, University of SriLanka. N.d.
- Mumbone, Mukendwa. *Innovations in Boundary Mapping: Namibia, Customary Land, and UAV's*. 2015.
- Naumann, M., Geist, M., Bill, R., Niemeyer, F., and Grenzdorffer, G. *Accuracy Comparison of Digital Surface Models Created by UAS Imagery and Terrestrial LASer Scanner*. Professorship for Geodesy and Geoinformatics. Universitat Rostock. 2013.
- Ohio Geographically Referenced Information Program. Retrieved from webpage: <http://ogrip.oit.ohio.gov/ProjectsInitiatives/OSIPDataDownloads.aspx>. 2017.
- Pix4D. *User Manual*. 2016.
- Schmid, H., *Error Theory of Intersection Photogrammetry*. Ballistic Research Laboratories, Report No. 785. 1951.
- Schmidt, Michael D. *Simulation and Control of a Quadrotor Unmanned Aerial Vehicle*. University of Kentucky. 2011.
- Singh, Ron, Artman, David, Taylor, David W., and Brinton, Dave. *Basic Surveying – Theory and Practice*. Oregon Department of Transportation. 2000.

Skidmore, Andrew K. A. *Comparison of Techniques for Calculating Gradient and Aspect from a Gridded Digital Elevation Model*. *Geographical Information Systems*. Vol. 3, No. 4. 1989.

T.M. Lillesand, & R.W. Kiefer, J.W. Chipman. *Remote Sensing and Image Interpretation, Sixth Edition*. John Wiley & Sons. Basic Principles of Photogrammetry.

US Patent Office, Patent Number 3,742,495. *Drone System Guidance and Method*. 1973.

US Patent Office, Patent Number 6,201,883. *Topography Measuring Device*. 2001.

Walker, Jeffery P., and Willgoose, Garry R. *A Comparative Study of Australian Cartometric and Photogrammetric Digital Elevation Model Accuracy*. *Photogrammetric Engineering and Remote Sensing*. Vol. 72, No. 7. July 2006.

Warner, Timothy A. and Campagna, David J. *Remote Sensing with IDRISI Taiga: A Beginner's Guide*. Geocarto International Centre. 2009.

Wolf, Paul R., and Ghilani, Charles D. *Elementary Surveying: An Introduction to Geomatics*. 1st Edition. 1997.

Wolf, Paul R., and Ghilani, Charles D. *Adjustment Computations: Statistics and Least Squares in Surveying and GIS*. 10th Edition. 2002.

Zukowskyj, Paul, Teeuw, Richard, and Munro, Oliver. *Interpolated Digital Elevation Models, Differential Global Positioning System Surveys and Digital Photogrammetry: A Quantitative Comparison of Accuracy from a Geomorphological Perspective*. n.d.

Zhang, Weihua, and Montgomery, David R. *Digital Elevation Model Grid Size, Landscape Representation, and Hydrologic Simulations*. *Water Resources Research*, Vol. 30, No. 4, April 1994.

Appendix A Tables and Maps

Table 1 GCP report for error accuracy

| | | | |
|-----------------------|----------|----------|----------|
| Mean (ft) | 0.000000 | 0.000000 | 0.000000 |
| Sigma (ft) | 1.245790 | 1.632082 | 1.903370 |
| RMS Error (ft) | 1.245790 | 1.632082 | 1.903370 |

Table 2 GCP comparison chart

| OID | Y | X | Z | DESCRIPTION | LOCATION |
|------------|------------|-------------|----------|--------------------|-----------------|
| 2 | 747715.55 | 2331115.96 | 1178.65 | TARGET | DICKINSON |
| 3 | 748059.06 | 2330924.42 | 1154.17 | TARGET | DICKINSON |
| 101 | 705680.958 | 2318898.293 | 1227.434 | TARGET | TALLGRASS |
| 104 | 705093.26 | 2319151.93 | 1231.191 | TARGET | TALLGRASS |
| 203 | 754124.29 | 2360173.614 | 1226.729 | TARGET | ASPHALT |
| 207 | 754451.195 | 2359674.005 | 1228.093 | TARGET | ASPHALT |

Table 3 Inverse report derived from Trimble Office.

| From | To | Geodetic Azimuth | Ellipsoid Distance | Grid Azimuth | Grid Distance (US survey foot) | Ground Distance (US survey foot) | Elevation (US survey foot) |
|-------------|-----------|-------------------------|---------------------------|---------------------|---------------------------------------|---|-----------------------------------|
| 207 | 1007022 | 69°06'14" | 0.552 | 69°06'14" | 0.552 | 0.552 | 0.004 |
| 207 | 622296 | 332°00'37" | 0.612 | 332°00'37" | 0.612 | 0.612 | 0.064 |
| 207 | 517380 | 43°29'52" | 1.43 | 43°29'52" | 1.43 | 1.43 | 0.977 |
| 207 | 1007122 | 204°03'05" | 0.459 | 204°03'05" | 0.459 | 0.459 | 0.012 |
| 207 | 517302 | 232°53'25" | 4.971 | 232°53'25" | 4.971 | 4.971 | 0.727 |
| 207 | 518614 | 348°10'10" | 9.175 | 348°10'10" | 9.175 | 9.175 | 1.007 |

Table 4 LiDAR report char

| PNT RCRD | INTENSITY | NO RTRNS | CLASS CODE | X | Y | Z | GPS TIME | LAS REF |
|----------|-----------|----------|------------|-----------|-----------|---------|-----------|----------|
| 323663 | 157 | 1 | 2 | 2331118.5 | 747713.38 | 1179.2 | 60814.988 | s2330745 |
| 322767 | 173 | 1 | 2 | 2331111.3 | 747722.5 | 1178.77 | 60814.956 | s2330745 |
| 323664 | 171 | 1 | 2 | 2331109.9 | 747714.34 | 1180.2 | 60814.988 | s2330745 |
| 296348 | 61 | 1 | 2 | 2330926.2 | 748061.54 | 1149.19 | 60813.683 | s2330745 |
| 296347 | 144 | 1 | 2 | 2330917.8 | 748062.37 | 1149.71 | 60813.716 | s2330745 |
| 297177 | 80 | 1 | 2 | 2330924.9 | 748052.85 | 1150.5 | 60813.716 | s2330745 |
| 517380 | 158 | 1 | 2 | 2359675 | 754452.23 | 1229.07 | 343955.14 | s2355750 |
| 517302 | 204 | 1 | 2 | 2359670 | 754448.2 | 1228.82 | 343955.13 | s2355750 |
| 518614 | 82 | 1 | 2 | 2359672.1 | 754460.18 | 1229.1 | 343955.18 | s2355750 |
| 150418 | 128 | 1 | 2 | 2360174.4 | 754121.62 | 1226.14 | 341947.31 | s2355750 |
| 149344 | 180 | 1 | 2 | 2360177.9 | 754130.16 | 1226.17 | 341947.28 | s2355750 |
| 149343 | 195 | 1 | 2 | 2360170.2 | 754131.67 | 1226.65 | 341947.28 | s2355750 |
| 652271 | 207 | 1 | 2 | 2319150.1 | 705097.4 | 1229.95 | 236034.27 | s2315705 |
| 652272 | 180 | 1 | 2 | 2319160.1 | 705095.19 | 1230.15 | 236034.27 | s2315705 |
| 651957 | 189 | 1 | 2 | 2319148.4 | 705101.44 | 1230.2 | 236034.25 | s2315705 |
| 628767 | 212 | 1 | 2 | 2318899.7 | 705682.33 | 1219.49 | 236032.13 | s2315705 |
| 628766 | 209 | 1 | 2 | 2318891.1 | 705684.5 | 1220.63 | 236032.13 | s2315705 |
| 629042 | 183 | 1 | 2 | 2318900 | 705675.2 | 1220.54 | 236032.16 | s2315705 |

Table 5 Absolute camera and deviation uncertainties

| | X (ft) | Y (ft) | Z (ft) | Omega (degree) | Phi (degree) | Kappa (degree) |
|--------------|--------|--------|--------|----------------|--------------|----------------|
| Mean | 0.23 | 0.22 | 0.48 | 0.043 | 0.052 | 0.015 |
| Sigma | 0.06 | 0.06 | 0.14 | 0.006 | 0.014 | 0.006 |

Table 6 Relative geolocation variance report

| Relative Geolocation Error | Images X [%] | Images Y [%] | Images Z [%] |
|---|--------------|--------------|---------------------|
| [-1.00, 1.00] | 99.38 | 100.00 | 99.07 |
| [-2.00, 2.00] | 100.00 | 100.00 | 100.00 |
| [-3.00, 3.00] | 100.00 | 100.00 | 100.00 |
| Mean of Geolocation Accuracy (ft) | 5.00 | 5.00 | 10.00 |
| Sigma of Geolocation Accuracy (ft) | 0.00 | 0.00 | 0.00 |
| Geolocation Orientational Variance | | | RMS [degree] |
| Omega | | | 0.96 |
| Phi | | | 0.58 |
| Kappa | | | 5.27 |

Table 7 Asphalt random samples

| OID | Y | X | Z | DESCRIPTION |
|---------|------------|-------------|-------------|-------------|
| 208 | 754285.301 | 2359710.95 | 1230.703 | TARGET |
| 1544815 | 754285.376 | 2359710.805 | 1230.405 | LAS |
| 1206500 | 754285.264 | 2359711.104 | 1230.72 | LAS |
| 805391 | 754284.911 | 2359710.797 | 1230.61 | LAS |
| 496606 | 754285.87 | 2359709.06 | 1232.92 | LIDAR |
| | | Z Mean: | 1230.578333 | |
| | | Z SD: | 0.086666667 | |

Table 8 Dickinson random samples

| OID | Y | X | Z | DESCRIPTION |
|------------|------------|-------------|----------|--------------------|
| 3 | 748059.064 | 2330924.416 | 1154.171 | TARGET |
| 483030 | 748058.894 | 2330923.95 | 1154.181 | LAS |
| 94555 | 748059.542 | 2330924.655 | 1154.106 | LAS |
| 32067 | 748058.792 | 2330925.213 | 1154.163 | LAS |
| 296348 | 748061.53 | 2330926.07 | 1149.19 | LIDAR |
| | | Z Mean: | 1154.15 | |
| | | Z SD: | 0.022 | |

Table 9 Tallgrass Random Samples (A)

| OID | Y | X | Z | DESCRIPTION |
|------------|------------|-------------|-------------|--------------------|
| 109 | 705265.124 | 2318852.466 | 1225.284 | TARGET |
| 3326 | 705265.754 | 2318853.633 | 1225.154 | LAS |
| 980 | 705258.406 | 2318853.791 | 1225.08 | LAS |
| | | Z Mean: | 1225.172667 | |
| | | Z SD: | 0.055666667 | |

Table 10 Tallgrass Random Samples (B)

| OID | Y | X | Z | DESCRIPTION |
|-------|-------------|-------------|----------|-------------|
| 106 | 2318991.437 | 704757.168 | 1228.376 | TARGET |
| 10362 | 704756.878 | 2318994.019 | 1228.627 | LAS |
| 5521 | 704762.027 | 2318987.276 | 1228.32 | LAS |
| | | Z Mean: | 1228.441 | |
| | | Z SD: | 0.093 | |

Table 11 Deviation report

| POINT RECORD | Y | X | Z | PARENT LOCATION A Sample |
|---|-------------------------------|-------------|------------|----------------------------|
| 150419 | 754123.146 | 2360166.87 | 1226.33 | s2360750 |
| 844333 | 754123.949 | 2360165.654 | 1226.517 | Asphalt Results Tracks 2 |
| 817224 | 754122.973 | 2360168.931 | 1226.495 | Asphalt Results Tracks 2 |
| 150435 | 754120.303 | 2360165.437 | 1226.56 | s2360750 |
| | <i>Average of the samples</i> | | 1226.4755 | |
| <i>Average deviation of the samples</i> | | | | 0.07275 |
| POINT RECORD | Y | X | Z | PARENT LOCATION B Sample |
| 61994 | 747760.881 | 2330755.766 | 1212.1 | s2330745 |
| 701060 | 747760.291 | 2330753.544 | 1212.553 | Dickinson Results Tracks 2 |
| 701164 | 747763.225 | 2330753.822 | 1212.487 | Dickinson Results Tracks 2 |
| 701252 | 747763.225 | 2330758.613 | 1212.067 | Dickinson Results Tracks 2 |
| | <i>Average of the samples</i> | | 1212.30175 | |
| <i>Average deviation of the samples</i> | | | | 0.21825 |

Table 12 Root Mean Square/Altitude relationship table (Source: ASPRS 2015)

| Altitude (m) | Positional RMSEr (cm) | Altitude (m) | Positional RMSEr (cm) |
|--------------|-----------------------|--------------|-----------------------|
| 500 | 13.1 | 3000 | 41.6 |
| 1000 | 17.5 | 3500 | 48 |
| 1500 | 23 | 4000 | 54.5 |
| 2000 | 29 | 4500 | 61.1 |
| 2500 | 35.2 | 5000 | 67.6 |

Table 13 USGS check shot point:

| Job: ASPH_GCP | Version:12.50 | Units: US Survey Feet | Elevation | Description |
|---------------|---------------|-----------------------|-----------|--------------------|
| FREO | 804303.239 | 2315483.787 | 1011.685 | VRS CORS Station |
| 21 | 754323.051 | 2366807.185 | 1295.349 | USGS MONUMENT E-64 |
| 22 | 754323.089 | 2366807.154 | 1295.378 | USGS MONUMENT E-64 |

Table 14 LAS points derived from UAS:

| POINT_RECORD | X | Y | Z | LOCATION |
|---------------------|-------------|------------|----------|-----------------|
| 247183 | 2319152.886 | 705093.397 | 1231.15 | TALLGRASS |
| 242670 | 2319151.215 | 705092.345 | 1231.31 | TALLGRASS |
| 147362 | 2319151.28 | 705093.679 | 1231.239 | TALLGRASS |
| 91755 | 2318898.821 | 705679.948 | 1227.51 | TALLGRASS |
| 86905 | 2318896.981 | 705680.937 | 1227.501 | TALLGRASS |
| 80333 | 2318899.043 | 705682.934 | 1227.163 | TALLGRASS |
| 442028 | 2331115.893 | 747715.521 | 1177.104 | DICKINSON |
| 441971 | 2331116.207 | 747715.697 | 1178.246 | DICKINSON |
| 445941 | 2331116.096 | 747715.444 | 1178.482 | DICKINSON |
| 477674 | 2330924.348 | 748059.049 | 1154.134 | DICKINSON |
| 94555 | 2330924.655 | 748059.542 | 1154.106 | DICKINSON |
| 32067 | 2330925.21 | 748058.792 | 1154.163 | DICKINSON |
| 1007122 | 2359673.818 | 754450.776 | 1228.105 | ASPHALT |
| 622296 | 2359673.718 | 754451.735 | 1228.157 | ASPHALT |
| 1007022 | 2359674.521 | 754451.392 | 1228.097 | ASPHALT |
| 1681069 | 2360173.719 | 754124.315 | 1226.497 | ASPHALT |
| 1665724 | 2360173.084 | 754124.041 | 1226.742 | ASPHALT |
| 1278052 | 2360173.372 | 754124.781 | 1226.682 | ASPHALT |

Table 15 Data Sources

| REQUIRED DATA | LOCATION | | SOURCE | STATUS |
|--|-------------------------------|-------------|------------------|------------------------------------|
| Images for Asphalt Plant | 40.062264° | -81.101547° | UAS | Collected and processed |
| Images for Dickinson Stock Lake | 40.046282° | -81.204402° | UAS | Collected and processed |
| GCP for Compressor Site | placed throughout project | | Trimble GPS | Collected and processed |
| GCP for Asphalt Plant | placed throughout project | | Trimble GPS | Collected and processed |
| GCP for Dickinson Stock Lake | placed throughout project | | Trimble GPS | Collected and processed |
| LiDAR from OGRIP (Ohio Graphically Referenced Information Program) | Tile(s) S2315705 and S2315700 | | OGRIP | For Comp Plant |
| LiDAR from OGRIP (Ohio Graphically Referenced Information Program) | Tile(s) S2360750 and S2355750 | | OGRIP | For Asphalt Plant |
| LiDAR from OGRIP (Ohio Graphically Referenced Information Program) | Tile(s) s2330745 | | OGRIP | For Lake |
| GPS As Built and Topo data from CAD | NAD 83 Ohio North State Plane | | Field Collection | CAD File - Collected and Processed |
| DEM from OGRIP - 1:24000 Tiles | Bethesda CA332 | | OGRIP | For Asphalt Plant |
| DEM from OGRIP - 1:24000 Tiles | Quaker City CK106 | | OGRIP | For Comp Plant |
| CAD file to process data | PC - AutoCAD Civil 3D | | | File |
| GIS file to correlate data | PC - ArcGIS 10.4.1 | | | File |



SHELLY SANDS ASPHALT STOCKPILE

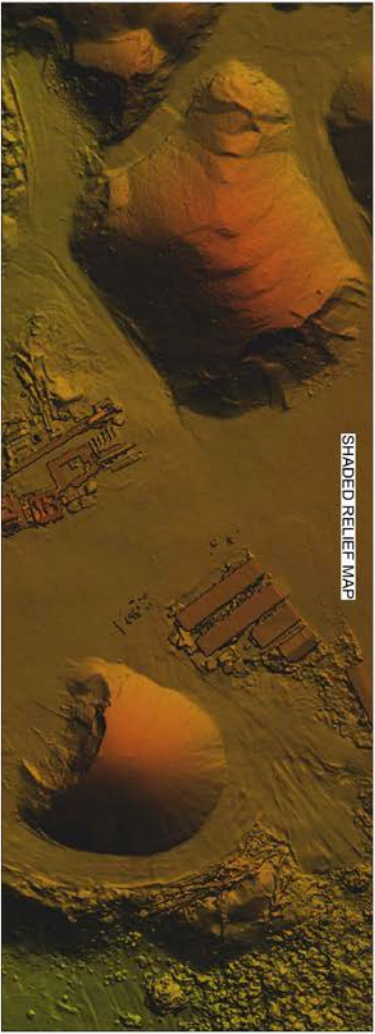
| INDEX | |
|-------------|-------------|
| A - 635,35 | H - 1327,77 |
| B - 3580,99 | I - 4343,88 |
| C - 889,40 | J - 453,06 |
| D - 633,80 | K - 1600,25 |
| E - 2705,36 | L - 118,99 |
| F - 4990,16 | M - 1582,86 |
| G - 124,40 | N - 2987,29 |

NOTE: VOLUME IN CUBIC YARDS.
NOTE: CALCULATIONS DERIVED FROM BAROMETRIC
ALTITUDE VIA UAV BASED ON WAD 93 ON SOUTH.



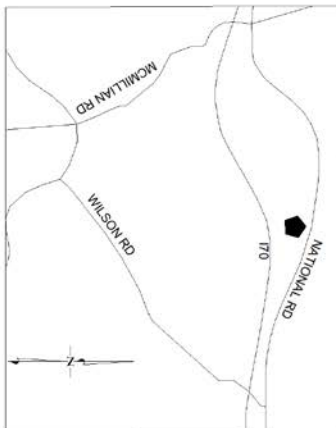
USC Domsife
Dana and David Domsife
College of Letters, Arts and Sciences
DATA AND MAP PREPARED AND COMPILED
BY CHARLES R. JORDEN, JR.
SEPTEMBER 2017

Figure 6 Asphalt site volume map.



**SHELLY SANDS
ASPHALT STOCKPILE
VOLUME CALCULATION**

LOCATION MAP



PROPERTY IS LOCATED WEST OF THE CITY OF SAINT CLAIRSVILLE IN THE STATE OF OHIO, IN THE COUNTY OF BELMONT. PROPERTY IS WEST OF THE CITY LIMITS ON NATIONAL ROADWAY 40 AT 10.9 MILES. DATA COMPILED WITH PERMISSION, AND IS COPYRIGHT OF THE AUTHOR.

USC Dornisite
Dana and David Dornisite
College of Letters, Arts and Sciences

DATA AND MAP DRAWN AND COMPILED BY USC DORNISITE IN SEPTEMBER 2017

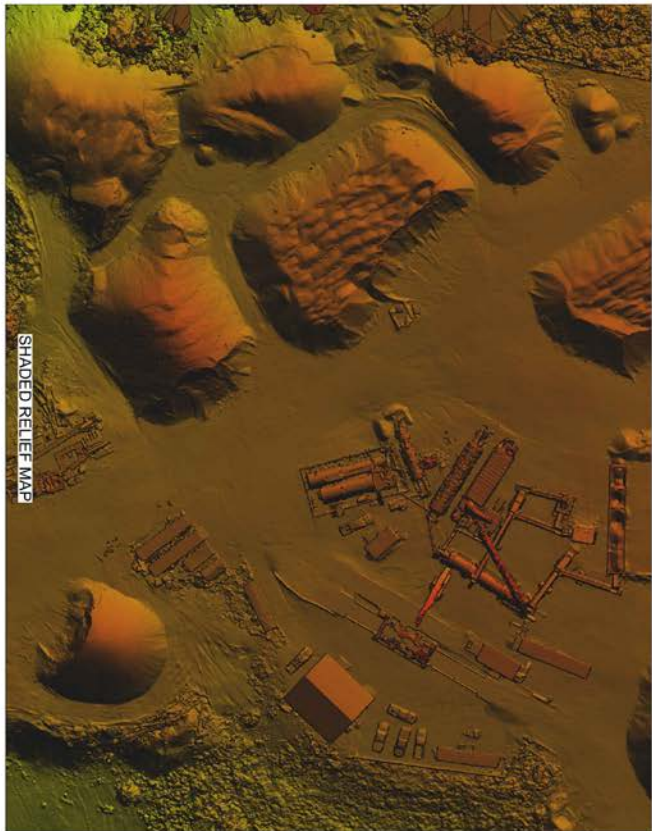
Figure 7 Asphalt site contour map – P 1



**SHELLY SANDS
ASPHALT STOCKPILE
VOLUME CALCULATION**

USC Dornsife
 Dana and David Dornsife
 College of Letters, Arts and Sciences
 DATA AND MAP PROVIDED COURTESY
 BY CHARLES R. JORDEN, JR.
 SEPTEMBER 2017

Figure 8 Asphalt site contour map – P 2



**SHELLY SANDS
ASPHALT STOCKPILE
VOLUME CALCULATION**

USC Dornsife
 Dana and David Dornsife
 College of Letters, Arts and Sciences
 DATA AND MAP DRAWN AND COMPILED
 BY CHRYSTOPHER J. WILSON
 SEPTEMBER 2017

Figure 9 Asphalt site contour map P 3

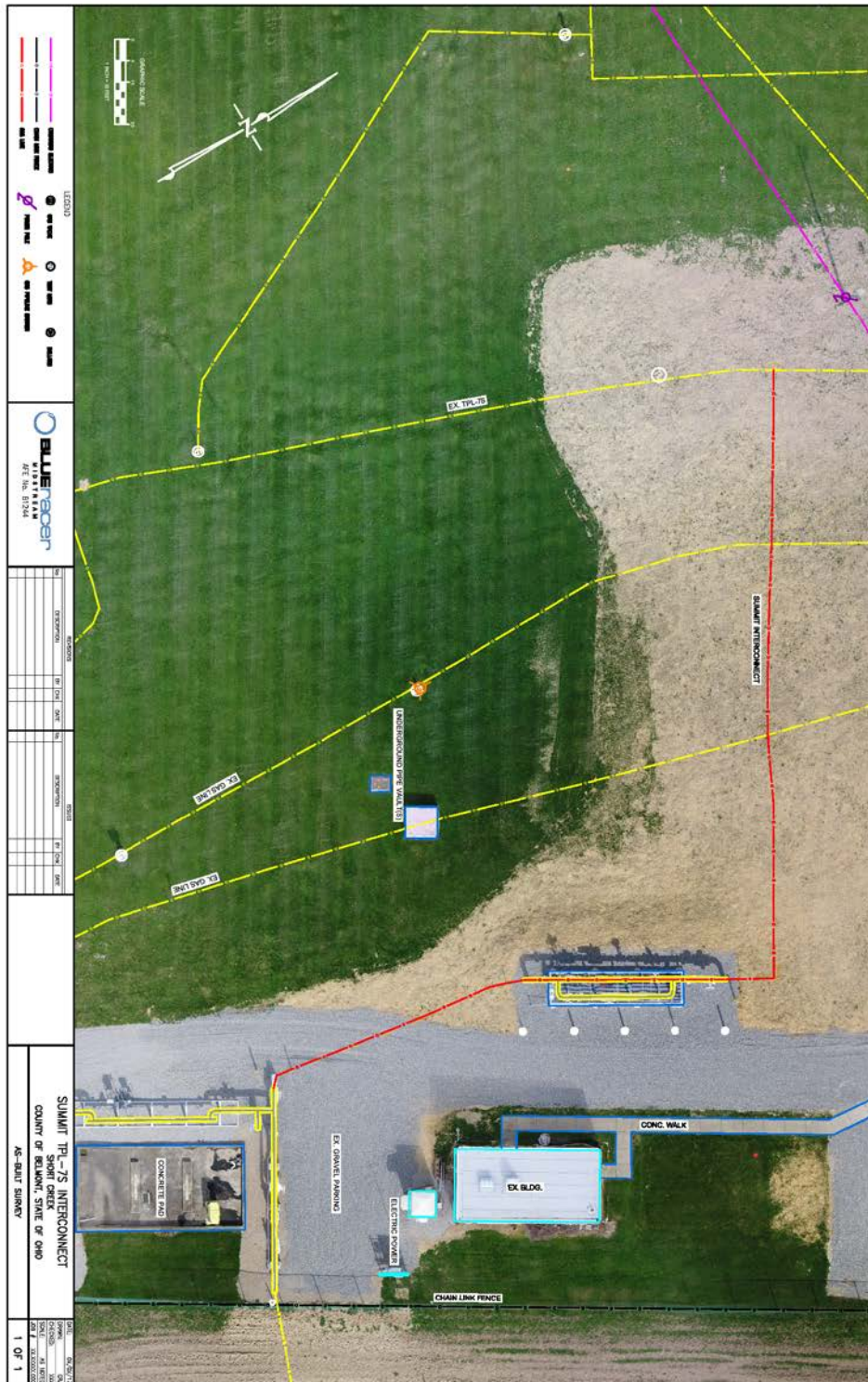


Figure 11 As-Built compilation report Price Pad P 2

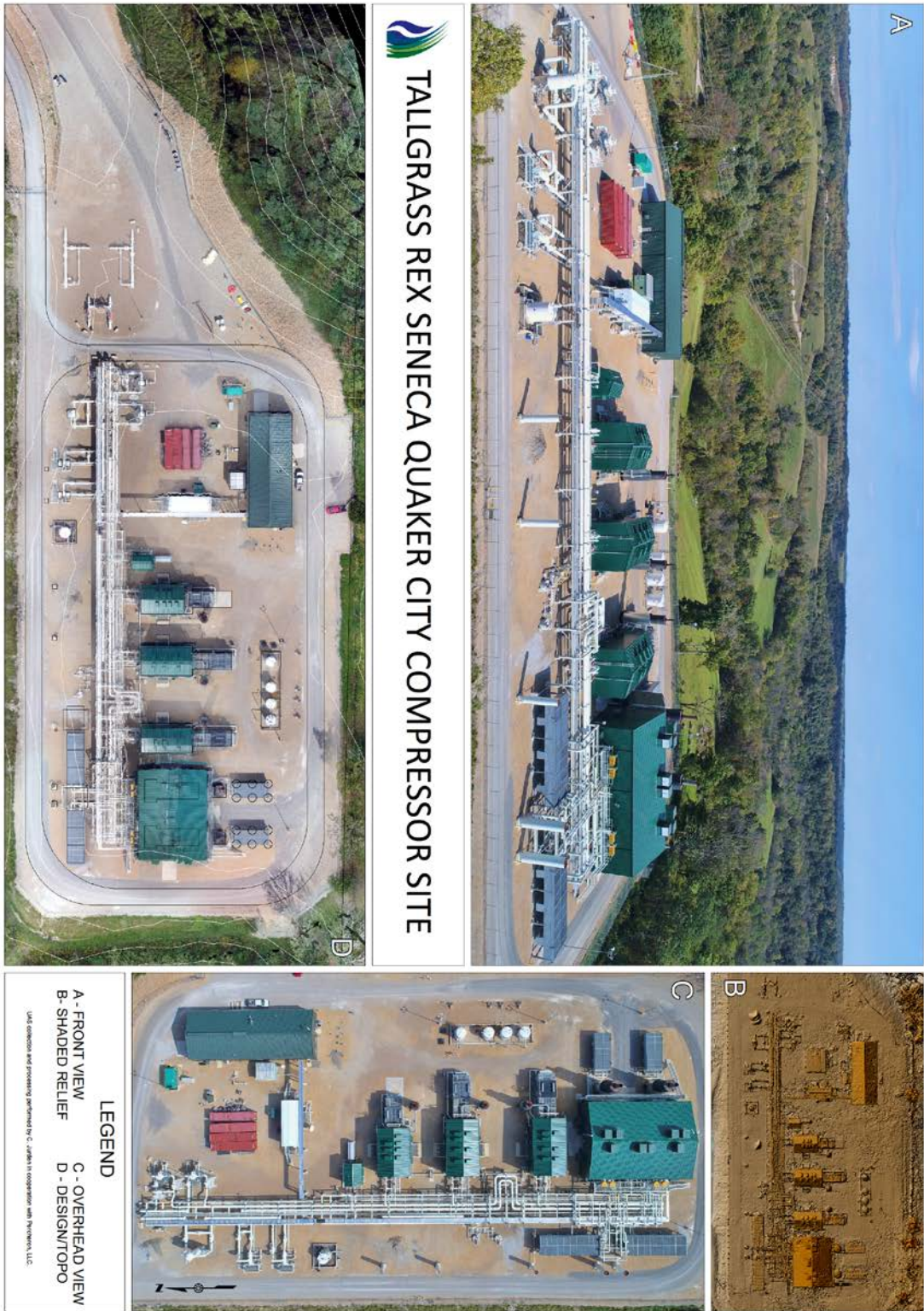
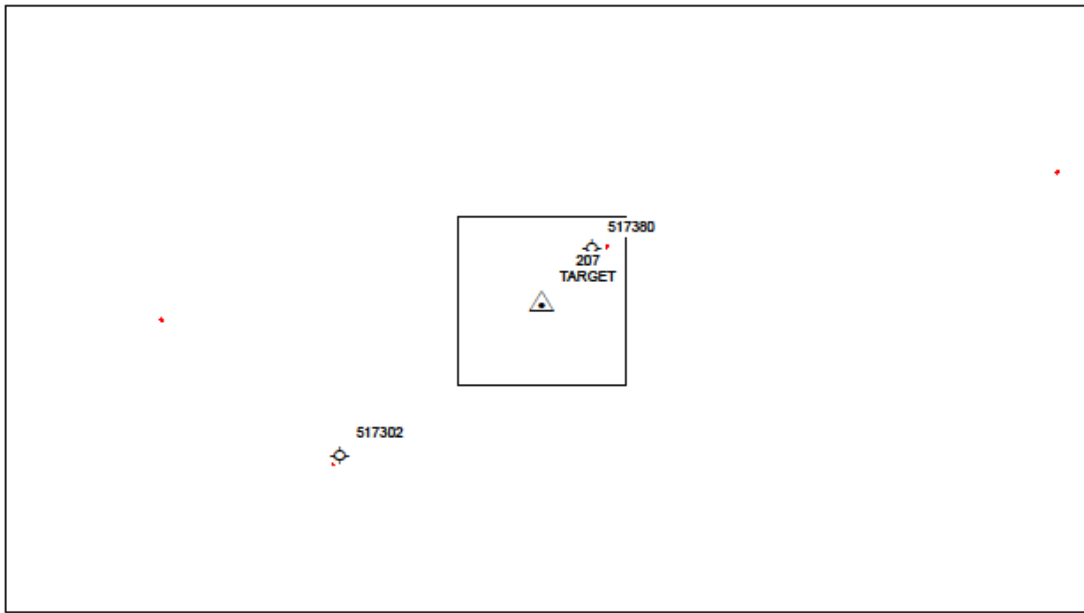
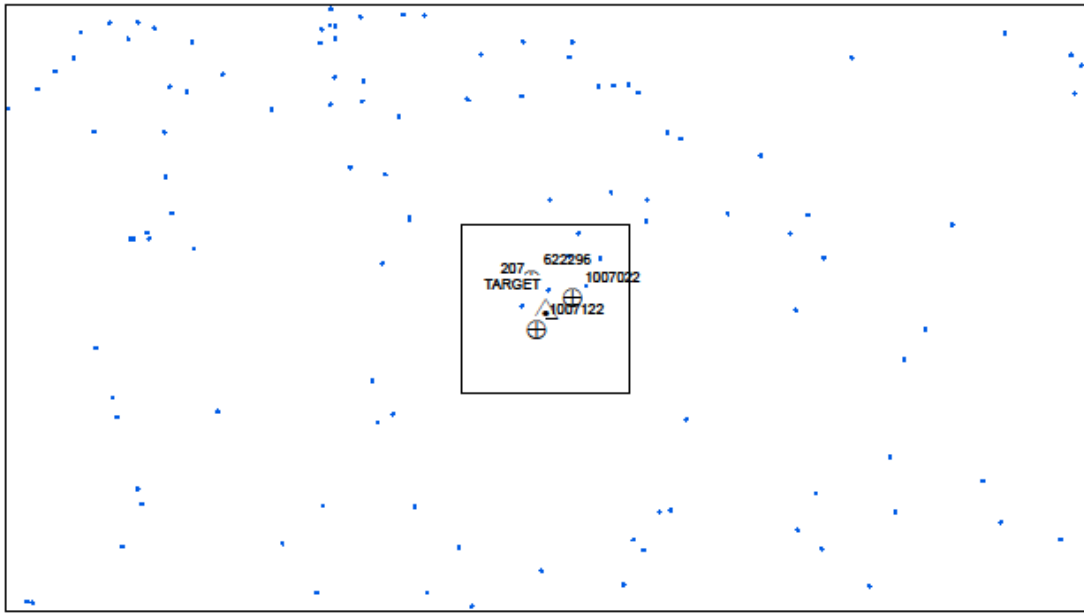


Figure 12 grass site As-built/UAS comparison map

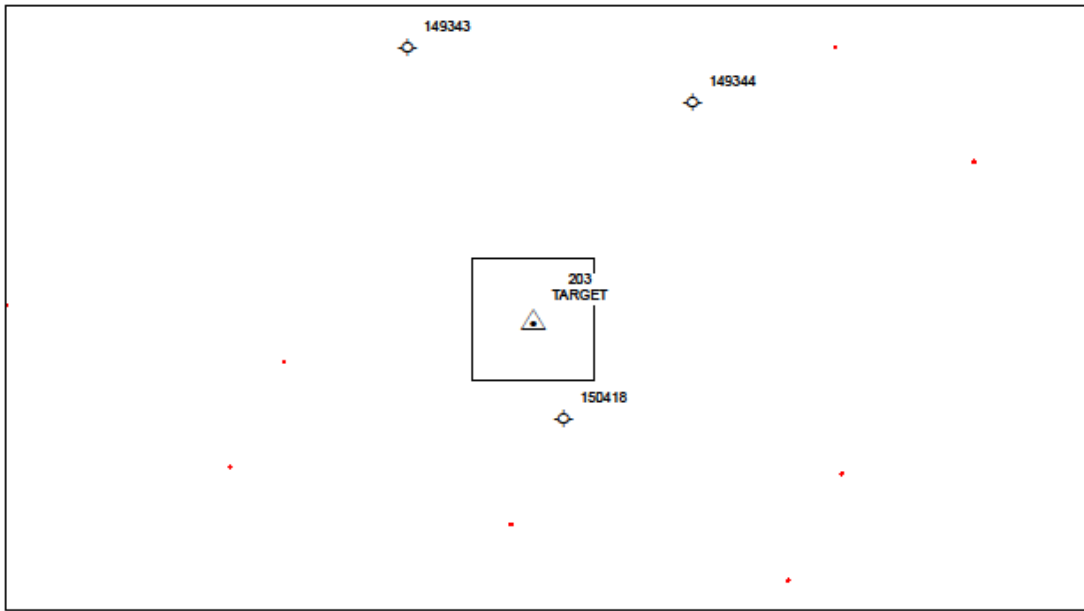


OGRIP LIDAR AND TARGET POINT
INSIDE A SQUARE METER PERIMETER

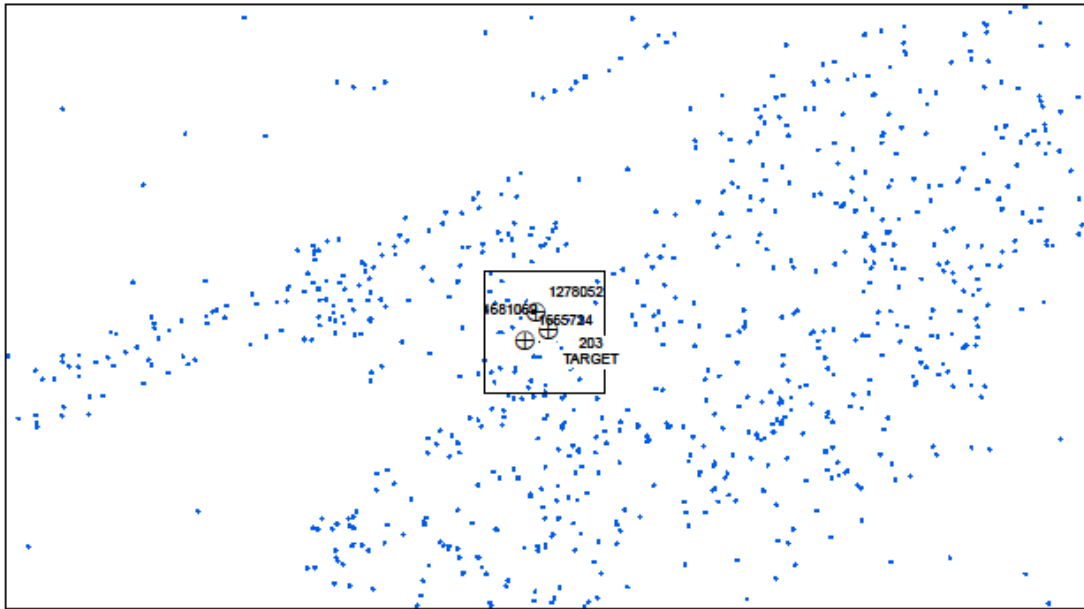


DRONE LAS AND TARGET POINT
INSIDE A SQUARE METER PERIMETER

Figure 13 LiDAR/LAS comparison Chart 1



OGRIP LIDAR AND TARGET POINT
INSIDE A SQUARE METER PERIMETER



DRONE LAS AND TARGET POINT
INSIDE A SQUARE METER PERIMETER

Figure 14 LiDAR/LAS comparison Chart 2